ELECTRICAL POWER GENERATION IN MICROBIAL FUEL CELLS USING CARBON NANOSTRUCTURE ENHANCED ANODES

Jennifer Lynn Lamp

Thesis Submitted to the Faculty of the Virginia Polytechnic Institute and State University in Partial Fulfillment of the Requirements for the Degree of:

MASTER OF SCIENCE

In

Mechanical Engineering

Committee Members:

Michael W. Ellis, Chair

Bahareh Behkam

Nancy G. Love

13 August 2009

Blacksburg, Virginia, USA

Keywords: microbial fuel cell, fuel cell, carbon nanostructures, MiFC, biofilm anode

ELECTRICAL POWER GENERATION IN MICROBIAL FUEL CELLS USING CARBON NANOSTRUCTURE ENHANCED ANODES

JENNIFER LYNN LAMP

ABSTRACT

Microbial fuel cells (MiFCs) have been suggested as a means to harness energy that is otherwise unutilized during the wastewater treatment process. MiFCs have the unique ability to treat influent waste streams while simultaneously generating power which can offset energy associated with the biological treatment of wastewater. During the oxidation of organic and inorganic wastes, microorganisms known as exoelectrogens have the ability to move electrons extracellularly. MiFCs generate electricity by facilitating the microbial transfer of these electrons from soluble electron donors in feedstocks to a solid-state anode.

While MiFCs are a promising renewable energy technology, current systems suffer from low power densities which hinder their practical applicability. In this study, a novel anode design using flame-deposited carbon nanostructures (CNSs) on stainless steel mesh is developed to improve the electron transfer efficiency of electrons from microorganisms to the anode and thus the power densities achievable by MiFCs. These new anodes appear to allow for increased biomass accumulation on the anode and may aid in the direct transfer of electrons to the anode in mediatorless MiFC systems. Experiments were conducted using anaerobic biomass in single-chamber MiFCs with CNS-enhanced and untreated stainless steel anodes. Fuel cells utilizing CNS-enhanced anodes generated currents up to two orders of magnitude greater than cells with untreated metal anodes, with the highest power density achieved being 510 mW m^{-2}.

ACKNOWLEDGEMENTS

There are many people I would like to thank for making this work possible. I would first like to thank my committee members: Dr. Nancy Love and Dr. Bahareh Behkam, and especially my adviser and committee chair, Dr. Michael Ellis for their help and support. I would also like to thank graduate students Jeremy Guest and Wendell Khunjar for their immense help with the microbiological aspect of this work as well as Dr. Ishwar Puri, Dr. Sayan Naha and Sonal Mazumder for manufacturing and providing information on carbon nanostructure-coated anodes. I would also like to thank Katie Radavich for her work during the summer of 2008, and Steve McCartney for aiding in obtaining the scanning electron microscope images taken during this study. Lastly, I would like to say thank you to my parents and siblings for their love and encouragement throughout my graduate studies at Virginia Tech.

DEDICATION

To Mom, Dad and Wendell.

PREFACE

The work in this thesis was conducted at Virginia Polytechnic and State University. It was funded in part by the Institute for Critical Technology and Applied Science (ICTAS) at Virginia Tech, the Water Environment Research Foundation (WERF) and the National Science Foundation (NSF). Any opinions, findings, and conclusions or recommendations expressed in this material are those of the author(s) and do not necessarily reflect the views of the National Science Foundation.

TABLE OF CONTENTS

LIST OF FIGURES

LIST OF TABLES

NOMENCLATURE

ac	acetate
AEM	anion exchange membrane
CNS	carbon nanostructure
COD	chemical oxygen demand
DMRB	dissimilatory metal-reducing bacteria
ED	electron donor
ESEM	environmental scanning electron microscope
GAC	granular activated carbon
GDL	gas diffusion layer
gl	glucose
MEA	membrane electrode assembly
MiFC	microbial fuel cell
OCV	open circuit voltage
PBS	phosphate buffered saline
PEM	proton exchange membrane
PEMFC	proton exchange membrane fuel cell
PFWWTP	Pepper's Ferry wastewater treatment plant
PTFE	polytetrafluoroethylene (Teflon®)
RVC	reticulated vitreous carbon
SEM	scanning electron microscope
SRT	solids retention time
SSM	stainless steel mesh

TCOD	total chemical oxygen demand
TEA	terminal electron acceptor
VSS	volatile suspended solids
WWTP	wastewater treatment plant

1.0 INTRODUCTION

Recent attention given to global climate change and the detrimental environmental effects of a fossil fuel based energy economy has led to increased interest in new, cleaner sources of energy. For a number of years, fuel cells have been one of the most promising of these renewable energy technologies. Proton exchange membrane fuel cells (PEMFCs) in particular seem promising for applications such as automobiles and portable power units. In most cases, PEMFCs use processed fuels (i.e. hydrogen or methanol) which react electrochemically with oxygen to produce power. A relatively new type of fuel cell known as a microbial fuel cell (MiFC) has the ability to produce power using microorganisms present in influent wastewater streams. MiFCs have the advantage over other types of fuels cells of using a fuel source that is readily available, without the need of additional refinement.

MiFCs have been proposed for a variety of small energy applications and in particular as a means to capture energy that is otherwise overlooked during the costly wastewater treatment process. While PEMFCs operate with power densities on the order of $3.0x10^6$-$10x10^6$ mW m^{-2} [2], the highest published power density of a MiFC is only $3.6x10^3$ mW m^{-2} [3]. Therefore, in order for MiFCs to be competitive with other energy technologies, vast improvements in power density need to be achieved.

Many different configurations of batch as well as continuous flow MiFCs have been studied, including single-chamber, double chamber, flat plate and upflow systems. The variety of MiFCs increases even more when one considers the material diversity which exists between studies of each these configurations. Design and material differences in anodes, cathodes, gas diffusion layers (GDL) and proton exchange membranes (PEM) can result in vast differences in

power output of MiFCs of otherwise similar design. As it is responsible for capturing the electrons deposited by microorganisms (or an electron shuttle), directly leading to current production, the anode is one of the most important and studied components of a MiFC. If improvements could be made to a MiFC anode which would increase its ability to allow for biofilm formation and direct electron transfer from microorganisms, perhaps great increases in power density could be realized.

This thesis focuses on the development of a new anode for a single-chamber MiFC, as well as a conduction-based model of the biofilm on the anode which predicts the power output of the fuel cells. Studies were conducted into the use of carbon nanostructure (CNS) enhanced stainless steel mesh as a material for MiFC anodes. Tests comparing the power production of batch, single-chamber, open-air cathode MiFCs utilizing CNS-enhanced and uncoated stainless steel mesh anodes were conducted using anaerobic sludge and glucose-based media. The model was based on an algorithm put forth by Andrew K. Marcus, Cesar I. Torres and Bruce E. Rittmann [4] which was adapted to match the properties of the MiFCs used in the present anode study.

The first chapter of this thesis will provide the reader with a brief introduction to how MiFCs produce electricity and the various microorganisms and materials used in the fuel cells, as well as the research objectives of this study. The second chapter is an overview of published literature on the topic of MiFCs. The third chapter outlines the experimental methods used to grow the microbial cultures, construct the anodes and test the batch MiFCs. Chapter 4 outlines the methods used in developing a computational model. Chapter 5 summarizes the results of MiFC testing and the computational model, and Chapter 6 discusses conclusions and future work.

1.1 MICROBIAL FUEL CELL BASICS

Microbial fuel cells operate by utilizing exoelectrogenic microorganisms (those which have the ability to transfer electrons outside of the cell) to transfer electrons from an electron donor in an influent feed to an insoluble electron acceptor (the anode). The multiple processes of electron transfer, as well as the path of electrons and protons in a batch, single-chamber MiFC are outlined in **Figure 1.1** below.

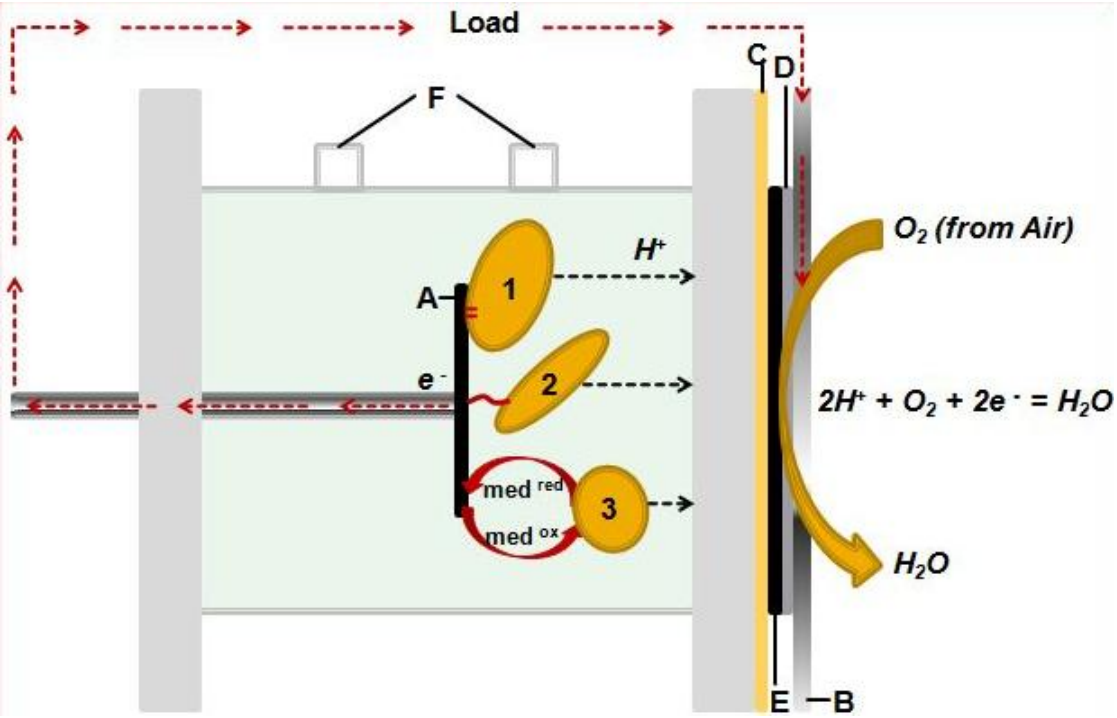

Figure 1.1. A schematic of a batch, single-chamber MiFC. Microorganisms deposit electrons on the anode (A) by direct electron transfer via membrane bound cytochromes (1), through the use of bacterial nanowires (2) and/or through interaction with a chemical mediator (3). These electrons flow through the circuit to a conducting plate (B) where they meet with hydrogen ions migrating through the proton exchange membrane (C) and oxygen diffusing from the air through a gas diffusion layer (D) at the platinum catalyst layer (E) where they react to make water. Two sampling ports (F) allow for the addition/removal of fluid during batch operation.

1.2 MICROBIAL FUEL CELL COMPONENTS

Though there are a multitude of different MiFC assemblies which have been studied, a few main hardware components are found in almost all configurations. Among these are the anode, proton exchange membrane (PEM), catalyst layer and gas diffusion layer (GDL).

1.2.1 ANODE

The anode is responsible for capturing electrons provided by the microorganisms contained within a MiFC. As the microorganisms oxidize a substrate, electrons are produced which the cell ultimately transforms to chemical energy in the form of ATP. These electrons move through respiratory enzymes and are released to a terminal electron acceptor (TEA) [5]. In a MiFC, these electrons first need to travel to the anode and through a completed circuit to reach the TEA (oxygen in this study) at the cathode. The anode must be chemically stable in the MiFC environment, as well as biologically compatible with the microorganisms with which it interacts. The anode must also be electrically conductive in order to complete the circuit necessary to produce a current. Materials which meet these requirements and have been studied for their use as MiFC anodes include carbon-based materials (graphite rods, brushes and granules, carbon clothes and papers) and steel (stainless steel meshes). These materials have been used in a variety of configurations and geometries in previous studies which are reviewed in Section 2.4.

1.2.2 PROTON EXCHANGE MEMBRANE, CATALYST LAYER AND CATHODE

The proton exchange membrane (PEM) serves as a barrier to gases like oxygen, while allowing for the conduction of hydrogen ions (protons) across its width. A PEM is found in the vast majority of fuel cells in use today, and is also a component in many MiFCs. In a single-

chamber, open air MiFC (similar to the fuel cell used in the ensuing studies) the PEM allows for the conduction of protons provided by microorganisms in the main chamber, while preventing oxygen from entering the chamber. If a significant flux of oxygen was allowed to permeate the inner chamber of the MiFC, a variety of problems could arise. If the fuel cell was being powered by anaerobic microorganisms, the presence of oxygen could significantly hinder their growth or inactivate the culture. On the other hand, if the microbial culture is one which normally utilizes oxygen as a terminal electron acceptor in nature, the presence of oxygen could disrupt electron transport to the anode and significantly decrease power density. The ion conducting polymer Nafion® (Dupont Co.) is the most commonly used PEM material for MiFCs; however, other materials have been used including anion exchange membranes and ultrafiltration membranes.

In many single-chamber, open-air MiFCs, a catalyst layer is painted onto the PEM (normally painted on the air-facing side of the PEM only) to form a cathode. In these MiFCs, oxygen (from the ambient environment), protons (passing through the electrolyte) and electrons (passing through the external circuit) react electrochemically on the catalyst layer to form water. Platinum is the most commonly used catalyst material in these systems. In two-chamber systems (those in which the anode and cathode are contained in separate compartments) materials such as carbon paper or graphite serve as electrodes, while the PEM is placed between the two chambers for proton transport.

1.2.3 GAS DIFFUSION LAYER

A gas diffusion layer (GDL) is normally used in open-air MiFCs which rely on the presence of oxygen in the ambient air to produce power. The GDL is also a common component of PEMFCs and is placed adjacent to the catalyst layer in order to diffuse gases evenly across the

catalyst layer while transferring current to the current collector (a stainless steel plate). Carbon cloth is commonly used as a material for GDLs.

1.3 RESEARCH OBJECTIVES

In this work we employ single-chamber MiFCs similar to **Figure 1.1**. The chambers of the MiFCs were constructed from polycarbonate and have a stainless steel mesh anode (either plain or coated with carbon nanostructures), a Nafion proton exchange membrane with a platinum catalyst layer painted on the air-facing side (0.4 mg-Pt cm^{-2}), and a carbon cloth gas diffusion layer. They were operated in fed-batch mode during experimental studies.

The research objectives of this work are as follows:

1. Attempt to produce current through a microbial fuel cell powered by microorganisms present in anaerobic digesters.
2. Determine whether the addition of carbon nanostructures to a MiFC anode can improve the power generation of microbial fuel cells.
3. Create a numerical model which can be used to describe empirical observations of successful power production in microbial fuel cells used in this study, thus providing a greater understanding of the phenomena occurring in MiFCs.

2.0 LITERATURE REVIEW

2.1 EARLY HISTORY

Microbial fuel cells (MiFCs) have been suggested as a means to harness energy that is otherwise unused from the wastewater treatment process. Bacteria have the ability to generate electrical current during their normal metabolic processes, which can be harnessed in the form of MiFCs and used to offset the costs associated with the biological treatment of wastewater.

In 1911, M.C. Potter first noted the ability of microorganisms to produce an electromotive force during the decomposition of organic matter. Experimenting with metallic electrodes and an apparatus specially designed for the biological experiment, he found that a pure culture of the bacterium *Bacillus coli communis* as well as yeast, could produce voltages on the order of 0.3 to 0.5 volts [6]. J.B. Davis and H.F. Yarbrough Jr. were the first to harness the electrical power of microbes in a fuel cell arrangement in the early 1960s. Using *Escherichia coli* (*E. coli*), *Nocardia* and glucose oxidase, they were able to produce electrical energy with a glucose substrate. Their MiFC consisted of two half-cells – one containing the bacteria, substrate and a platinum anode bubbled with nitrogen, the other containing a platinum cathode bubbled with oxygen connected to the former via a compartment housing a semi-permeable membrane [7]. These early experiments provided a basis for future research into the use of microbial systems for electrical power generation.

2.2 BIOLOGICAL ELECTRON TRANSFER AND MIFC BASICS

Many microorganisms use respiration as a means to produce energy-rich compounds such as adenosine triphosphate (ATP). During the normal respiration process, bacteria undergo a

series of oxidation and reduction reactions during which electrons are traded between electron donors and accepters and hydrogen ions (protons) are produced [8]. Exoelectrogens are a specific subset of bacteria that have the ability to transfer electrons to acceptors located outside of the cell. These exoelectrogenic bacteria enable a MiFC to produce power by transferring electrons during respiration to an anode instead of the usual terminal electron acceptor (TEA) [5]. An electrochemical potential which exists between the respiratory enzyme and the electron acceptor located at the cathode facilitates the flow of electrons from the anode and creates current [9]. In the case of many bacterial species, oxygen is the TEA and therefore must be separated from the compartment where biological substrate oxidation is occurring in order to maximize electron transfer to the anode. This is usually accomplished using a proton exchange membrane such as Nafion® which allows protons to pass through to the cathode chamber, but inhibits the diffusion of oxygen into the anode chamber.

Multiple mechanisms for electron transfer from the bacterial cell to the anode of a MiFC have been documented. These include transfer via a chemical mediator or shuttle, direct electron transfer and transfer along nanowires attached to certain microbial cells [10]. Chemical mediators are compounds that have the ability to be reduced by microorganisms as they shuttle electrons to the anode of a MiFC where they are oxidized as they deposit electrons. In some MiFCs these mediators can significantly increase electricity generation. Some chemical mediators that have been shown to improve MiFC electricity generation include neutral red [11, 12], AQDS [13] and thionin [12]. In an anaerobic MiFC containing a glucose substrate, *E. coli* and *Actinobacillus succinogenes* have been shown to produce current in a MiFC using neutral red or thionin as a chemical mediator [12]. Some species of dissimilatory metal-reducing bacteria or DMRB utilize such naturally occurring electron shuttles as humic substances which

are found in terrestrial and aquatic environments and are used during the anaerobic oxidation of organic matter [14], while other species like *Shewanella putrefaciens* have the ability to produce and excrete their own mediators [15]. The facultative anaerobe *Pseudomonas aeruginosa* was also found to excrete its own chemical mediator, pyocyanin, in order to perform electrochemical activities [16].

Additional studies using *Shewanella putrefaciens* by Kim et al. suggest that the bacterium has the ability to directly transfer electrons from each microbe to the anode through the use of proteins bound to the outer membrane of each cell known as cytochromes [17-19]. In nature, this microbe uses solid terminal electron acceptors such as iron during respiration (unlike many other organisms which use soluble electron acceptors) making it necessary for the bacterial cell to allow for a link across the outer membrane from the cytoplasmic membrane (where the electron transport chain is located) to these large, solid particles [20]. Cytochromes provide this link, and also make *Shewanella putrefaciens* a potential candidate for use in non-mediated MiFCs, as the anode used in the fuel cells is also a solid, insoluble, electron acceptor. Other organisms such as the metal-reducing anaerobe *Geobacter sulfurreducens* have also been found to produce electricity directly by attachment to an electrode [21].

Certain microorganisms such as *Shewanella oneidensis* (a DMRB), *Synechocystis* (a photosynthetic cyanobacterium) and *Pelotomaculum thermopropionicum* (a thermophilic fermentative bacterium) have been shown to produce electrically conductive appendages when in the presence of a scarce supply of terminal electron acceptors. These appendages resemble pili and are called bacterial nanowires [22]. Reguera et al. also found that a certain mutant of *Geobacter sulfurreducens* could connect to Fe(III) oxides through the use of highly conductive pili, which could be used for electron transfer [23].

2.3 MiFC Configurations

There are several ways in which to categorize MiFCs by reactor configuration. These fuel cells can first be classified by their flow operation – either continuous-flow or batch. Continuous-flow systems normally consist of a reactor containing the anode, cathode and microorganisms which has a continuous influent stream containing an electron donor such as glucose, acetate, butyrate, etc. and other vitamins which promote microbial growth. In a laboratory setting, this influent stream is often a carefully concocted media specifically aimed at supporting the particular microorganism(s) in the MiFC, while in real-world applications it would most likely be a wastewater stream. Batch systems, on the other hand, are not continually fed, and therefore must be fed at discrete times in order to stay in operation. These systems are more useful in laboratory experiments than in industrial applications.

Another general method of categorizing MiFCs is by chamber configuration. Most systems can be labeled as either single-chamber or two-chamber MiFCs. Single-chamber MiFCs are simpler and may be easier to operate than many two-chamber systems. Many of these MiFCs use cathodes exposed directly to the surrounding air thus negating the need for a separate chamber in which to contain the cathode.

2.3.1 Two-Chamber MiFCs

In two-chamber MiFCs, the anode and cathode are kept in discrete containers, separated by either a membrane or salt bridge. In many instances, a soluble cathodic electron acceptor is added or oxygen is introduced in the cathode chamber in order to increase reaction rates. A study by You et al. for example found that permanganate, hexacyanoferrate and oxygen could be used as electron acceptors in the cathodic chamber of a two-chamber MiFC. Using anaerobic

sludge and a medium of 600 mg COD L^{-1} glucose, the fuel cell produced powers of 116 mW m^{-2} (permanganate), 25.6 mW m^{-2} (hexacyanoferrate) and 10.2 mW m^{-2} (oxygen) [24]. In another study using hydrogen producing anaerobes, a two-chamber system using ferricyanide as a catholyte was found to produce more power and remove substrate more efficiently than an identical system using an aerated cathode chamber [25]. These studies imply that the use of soluble cathodic electron acceptors can increase the power and efficiency of MiFCs over the use of oxygen aeration. However, many of these compounds are toxic and if used in actual functioning systems, the effluent from these MiFCs would need to be treated before discharge (increasing costs and complexity), whereas aerated systems would be less likely to contain harmful substances.

A comparison between the use of a membrane and the use of a salt bridge for proton exchange between the two compartments has also been conducted. Using a pure culture of the anaerobe *Geobacter metallireducens*, the salt bridge system provided about one-twentieth the power density of the Nafion membrane system. This difference in power density was explained by the larger internal resistance of the salt bridge system [26].

Other studies into two-chamber MiFC systems include experiments using a low-pH catholyte chamber [27], and tests using cysteine as a substrate in an anaerobic, PEM system [28]. Wang et al. found that the start-up time for a two-chamber MiFC could be reduced by almost one-half by applying a positive poised potential to the anode, thus lessening the waiting time to achieve a steady current [29]. Another study determined that the oxygen diffusion into the MiFC could be decreased through the use of ferricyanide in the cathode chamber and by coating the original graphite anode with platinum [30].

2.3.2 TUBULAR AND UPFLOW MIFCS

Tubular and upflow MiFCs are alternative configurations being studied currently. Tubular MiFCs are generally cylindrical continuous-flow reactors with concentric compartments which house the anode and cathode. Lui et al. developed a tubular MiFC which consisted of a Plexiglas cylinder containing eight sandblasted graphite rods (acting as anodes) surrounding a cathode. The cathode was a carbon cloth coated with platinum hot pressed to a PEM which was then fused to the outside of a porous hollow tube. Ambient air flowed through the center of the porous cathode tube acting as the electron acceptor for the system. Using primary clarifier effluent from a domestic wastewater treatment plant as a biocatalyst, the system produced a maximum power density of 26 mW m^{-2} [31]. Scott et al. constructed a tubular MiFC out of two Nylon tubes – the smaller tube lined with carbon cloth served as the cathode and was inserted into the larger tube which was also lined with carbon cloth to serve as the anode. Small holes were drilled in the cathode tube to allow for ion transport, and air was pumped through the center of the tube as the electron acceptor. Using farm manure, this system was capable of producing 30 mW m^{-2} [32].

Two other research groups worked with continuous-flow tubular MiFCs using granular anodes. The first system consisted of a sturdy PEM rolled into a cylinder which was filled with graphite granules and inoculated with bacteria. The cathode (a woven graphite mat) was wrapped around the outside of the membrane and was dripped with a ferricyanide catholyte solution. Using a glucose-based feed which flowed through the anode compartment, the system achieved a maximum power output of 90 W m^{-3} (based on the net anode compartment volume) [33]. Similarly, the second group placed graphite granules into a plexiglas tube drilled with holes (anode) along with anaerobic sludge as the biocatalyst, while covering the outside of the

tube with a platinum-coated carbon cloth cathode. Also using a glucose-based feed, this system generated a maximum power of 50.2 W m^{-3} (based on the anode liquid volume) [34].

Upflow MiFCs are continuous-flow systems which pump influent media solutions upward through a granular anode. He et al. developed an upflow reactor which consisted of two cylindrical Plexiglas chambers stacked atop another, separated by a PEM. The lower container housed the reticulated vitreous carbon (RVC) anode, while the overlying chamber contained an RVC cathode (of smaller pore size). A sucrose based influent feed was fed upwards through the anode compartment and the effluent from the compartment was recirculated to mix with the influent stream. Using anaerobic sludge, and potassium hexacyanoferrate as a cathodic electron mediator, this system produced a maximum power of 170 mW m^{-2} based on the calculated surface area of the anode [35]. The same group also later studied an upflow MiFC which utilized a U-shaped cathode consisting of a PEM tube filled with granular activated carbon (GAC) inserted into a bed of GAC which served as the anode. Using anaerobic sludge and a sucrose-based feed, this system produced a maximum power of 29.2 W m^{-3} based on the wet volume of the anode [36]. Another study aimed at determining the fate of hydrogen gas in upflow MiFCs utilized a similar design to that of the first mentioned study by He et al. [37]

Another configuration, which has been studied by Min and Logan, is a continuus-flow, flat plate microbial fuel cell. Two polycarbonate plates with serpentine channels were bolted together to form cathode and anode chambers. The cathode was formed by carbon cloth containing a platinum catalyst (on one side) hot pressed to a piece of Nafion which was then placed on top of a carbon paper anode. Domestic wastewater was flowed through the anode channel, while air was passed through the cathode channel, resulting in an average power density of 72 mW m^{-2}. Using acetate in addition to the domestic wastewater allowed for a sustained

power generation of 286 mW m^{-2} [38]. This system is particularly interesting because of its ability to produce power with unaltered wastewater and compact design, which could allow for several of the reactors to be stacked together.

2.4 SINGLE-CHAMBER MiFCs

The focus of a majority of current research is aimed at single-chamber MiFCs as they are more applicable to practical operations. These MiFCs have only one fluid chamber which contains the biocatalyst, anode and substrate, and usually employs an air-cathode which uses the oxygen in the ambient atmosphere as a terminal electron acceptor to create current for the fuel cell. A brief summary of published experiments using single-chamber MiFCs is given in **Table 2.1** at the end of this chapter.

2.4.1 SINGLE-CHAMBER MiFCs: SUBSTRATES

There exists a wide range of substrates which have the ability to support electricity generation from single-chamber MiFCs. These include chemical substrates prepared in the laboratory designed to support specific microorganisms, wastewater-based substrates and combinations of both types.

Glucose is a common substrate, and studies using batch, single-chamber MiFCs (without a PEM) inoculated with domestic wastewater and fed with glucose, resulted in maximum power generations of 494 mW m^{-2} (600 mg L^{-1} glucose medium) [39], 766 mW m^{-2} (500 mg L^{-1} glucose medium) [40], 811 mW m^{-2} (500 mg L^{-1} glucose medium) [41], 480 mW m^{-2} (1000 mg L^{-1} glucose medium) [42] and 1430 mW m^{-2} (1000 mg L^{-1} glucose medium) [43]. Experiments on similarly designed fuel cells compared the power generation from membrane-free, single-

chamber MiFCs using acetate and butyrate-based substrates. The fuel cells were inoculated with domestic wastewater, and then fed a prepared substrate of either acetate or butyrate in varying amounts. The power generated from acetate-fed MiFCs were up to 66% higher than those fed with butyrate (506 mW m^{-2} versus 305 mW m^{-2}), implying that for microorganisms in wastewater streams, acetate may be a preferential electron donor to butyrate [44]. Another study found that six polyalcohols (xylitol, arabitol, ribitol, galactitol, mannitol and sorbitol) all could be used as carbon sources to power single-chamber MiFCs. The power densities ranged from 1490 to 2650 mW m^{-2}, with mannitol producing the lowest power density and galactitol producing the highest [45].

Other batch studies using acetate as an electron donor resulted in maximum power densities of 1330 mW m^{-2} (1000 mg L^{-1} acetate medium) [46], 1970 mW m^{-2} (1000 mg L^{-1} acetate medium) [47], 1460 mW m^{-2} (20-30 mM acetate medium) [48], 2011 mW m^{-2} (1000 mg L^{-1} acetate medium) [49], 728 mW m^{-2} (800 mg L^{-1} acetate medium) [50] and 2400 mW m^{-2} (1000 mg L^{-1} acetate medium) [43]. A fed-batch system running on 20 mM xylose produced 673 mW m^{-2} [51]. Although these aforementioned acetate-based MiFCs seem to have produced larger power densities than those using glucose, butyrate and xylose, the studies that resulted in these larger values were many times examining novel alterations to other fuel cell components which may be more responsible for the increased power generation than the type of electron donor substrate.

Continuous-flow single-chamber MiFCs can operate on similar substrates, often with increased performance. One study for example, found that when using a glucose-based substrate and continuous-flow reactor, the maximum power generated reached 1540 mW m^{-2}, while the

fed-batch system generated only 432 mW m^{-2} [41]. Acetate-based systems have produced 1800 mW m^{-2} [48], and a system using xylose produced 1093 mW m^{-2} (20 W m^{-3}) [51].

As previously mentioned, single-chamber MiFCs can also be fed with the electron donors already present in wastewater streams. Domestic wastewater has been used as a substrate in continuous-flow systems to produce power densities of 464 mW m^{-2} (15.5 W m^{-3}) [41]. Several studies have also explored the use of single-chamber MiFCs for the simultaneous treatment of and power generation from brewery wastewater. One such study used batch MiFCs operated at 20°C and 30°C and found that a maximum power density of 170 mW m^{-2} and 205 mW m^{-2} and a COD removal efficiency and 85% and 87% could be achieved respectively. With the addition of a 200mM phosphate buffer (PBS), the power density in a 30° reactor could be increased to 528 mW m^{-2} with an 86% COD removal efficiency [52]. A similar study using brewery wastewater with 50mM PBS found that a 20°C MiFC could produce 435 mW m^{-2} with a COD removal efficiency of 85%, while a 30°C MiFC could produce 483 mW m^{-2} with a COD removal efficiency of 87% [53]. A third study used a single-chamber MiFC operated at 20°C to produce 30 mW m^{-2} with a 56% COD removal efficiency [54].

Other substrates used in single-chamber MiFCs include paper recycling wastewater and swine wastewater. One study compared the power production and removal efficiency of total chemical oxygen demand (TCOD) between MiFCs using unamended and buffered paper recycling plant wastewater. The unamended substrate resulted in a peak power density and TCOD removal efficiency of 144 mW m^{-2} and 29%, while the addition of a 50mM PBS solution to the wastewater generated of 501 mW m^{-2} and removed 76% of the TCOD. Increasing the PBS solution to 100mM further increased the power generation of the fuel cells to 627 mW m^{-2} (a 245% improvement over the unamended wastewater substrate) [55]. These results, as well as

those from aforementioned studies using brewery wastewater [52, 53], indicate that the conductivity of substrates used in MiFCs has a large impact on power generation. A higher conductivity (achieved by the addition of PBS) results in a lower internal resistance in the fuel cells thereby allowing for larger power production. Another study used single-chamber, fed-batch MiFCs at 30°C to simultaneously remove greater than 84% of organic matter and 99.76% of odor-causing compounds while generating up to 228 mW m^{-2} of power from swine wastewater [56].

The variety of substrates, both laboratory-created media and wastewater streams, which can be used as electron donor sources in single-chamber MiFCs show the large range of applications of this new energy technology.

2.4.2 SINGLE-CHAMBER MIFCS: MEMBRANES AND CATHODES

The membrane and cathode structure of a single-chamber MiFC can have significant effects on power production and efficiency. Multiple studies have been conducted into the use of different cathode materials and catalysts, as well as into the use of membrane-less fuel cells.

Many cathode materials have been utilized in MiFCs, including carbon paper and carbon cloth. In single-chamber systems, the cathode is normally exposed directly to the air (an air-cathode), using the ambient oxygen as an electron acceptor. Catalysts such as platinum (Pt) are utilized with the electrodes in order to increase reaction rates.

One study found that by using a batch MiFC fed with acetate and an equal Pt loading, a carbon cloth cathode could produce a 68% higher power density than a carbon paper cathode [46]. Another study found that the application of polytetrafluoroethylene (PTFE) diffusion layers to the air-facing side of a carbon cloth air-cathode could improve the power density and

coulombic efficiency of the MiFC as well as decrease water loss through the cathode. Four coatings of PTFE resulted in a 71% increase in the coulombic efficiency (from 19% to 32%) and a 42% increase in the maximum power density (from 538 to 766 mW m^{-2}) [40].

Several studies have also been conducted into the type of catalyst used on the cathode in order to increase the rate of reaction. Cheng et al. for example examined different catalysts and polymer binders for their use in air-cathode, single-chamber MiFCs. Their experiments had three particularly interesting results: (1) Nafion solution was a better binder for Pt than PTFE, (2) reducing the Pt loading on the cathode from 0.5 mg cm^{-2} to 0.1 mg cm^{-2} only reduced the power output by 19% and (3) the use of an inexpensive cobalt material (cobalt tetramethylphenylporphyrin or CoTMPP) as a catalyst instead of Pt only resulted in a power density drop of 12% (from the 0.5 mg cm^{-2} Pt loading) [42]. Another study found that using iron phthalocyanine (FePc) as a cathode catalyst could produce a larger power density than platinum (634 versus 593 mW m^{-2}) [49]. These results show that only a small amount of expensive Pt catalysts need to be used in MiFCs, and that inexpensive catalysts like CoTMPP are a viable option which can lower the cost of operation.

Nafion is one of the most common materials used as a PEM in MiFCs, but other materials have been examined. Zuo et al. for example, compared the power density from batch, single-chamber MiFCs with graphite brush anodes using an anion exchange membrane (AEM), cation exchange membrane (CEM) and ultrafiltration membrane. They found that the AEM produced the highest power density at 449 mW m^{-2} when coated with a catalyst loading of 0.5 mg cm^{-2} CoTMPP. The use of a current collector and an increase in the solution conductivity resulted in an even larger power generation of 728 mW m^{-2} [50].

A membrane-less MiFC system is desirable because the PEM not only adds cost, but also increases the ohmic resistance of the fuel cell. Liu and Logan conducted experiments into the use of single-chamber MiFCs in the presence and absence of a proton exchange membrane. Using glucose, they found that the removal of the PEM increased power output from 262 to 494 mW m^{-2} while decreasing the coulombic efficiency from 40-55% to 9-12%. Similar results were found using wastewater with an increase in power from 28 to 146 mW m^{-2} and decrease in coulombic efficiency from 28% to 20% after removal of the PEM [39]. These results are attributed to the removal of the PEM increasing the cathode potential (thus increasing power) while allowing more oxygen to diffuse into the fuel cell (decreasing the coulombic efficiency). A later study found that using J-Cloth on the water-facing side of an air-cathode, membrane-less MiFC could increase the coulombic efficiency, while still providing a low internal resistance as expected in a membrane-less fuel cell. In fed-batch and continuous flow mode, 1120 mW m^{-2} (627 W m^{-3}) and 1800 mW m^{-2} (1010 W m^{-3}) were generated respectively, and the coulombic efficiency was increased from 35% (without J-Cloth) to 71% (with J-Cloth) [48].

2.4.3 SINGLE-CHAMBER MIFCS: ANODES

The anode is one of the most important parts of a MiFC. The anode must be conductive and compatible with the microorganisms which power the fuel cell. The geometric configuration, surface area, position and material composition of a MiFC anode all affect the overall fuel cell power production.

One study found that (using a carbon paper anode and cathode) the optimal anode-cathode spacing in a single-chamber, air-cathode MiFC was 2.0 cm. The power densities at distances of 4.0 cm and 2.0 cm resulted in power densities of 720 and 1210 mW m^{-2} respectively

[46]. A similar study found that further decreasing the anode-cathode spacing actually resulted in a decrease in power density. When altering the spacing from 2.0 cm to 1.0 cm during batch operation with glucose, the power density fell from 811 mW m^{-2} to 423 mW m^{-2}. This same study found that operating the reactor as a continuous-flow system with advective flow through a porous, carbon cloth anode toward the cathode and 1.0 cm anode-cathode spacing could significantly increase power density. Using a glucose-base substrate, the power density rose to 1540 mW m^{-2} [41]. These studies both show that the position of the anode, and not just the material or geometry, can have a significant impact on the performance of single-chamber MiFCs.

Using a fed-batch, air-cathode MiFC, Cheng and Logan found that a surface alteration to an otherwise plain carbon cloth anode could boost power production. Using an acetate-based substrate, they found that increasing the PBS concentration in the feed could increase the power density from to 1330 to 1640 mW m^{-2}, which was further increased to 1970 mW m^{-2} with an ammonia-gas anode treatment. These two alterations also resulted in a 30% reduction of the startup time of the MiFC [47]. Another study into the effect of anode surface alterations on the performance of batch, air-cathode MiFCs was completed by Scott et al. They compared the power generation in MiFCs using plain graphite felt anodes with that of MiFCs using altered graphite felt anodes. The control fuel cell (using a plain anode) produced 9.5 mW m^{-2}, while those with surface additions of nitric acid treated carbon (C/HNO_3), carbon/polyaniline/D-CSA composite (PANI/C), carbon nanofibres synthesized using polyaniline (PANI 900), Ketjen Black carbon (KjB) and PANI tubes generated 28.4, 26.5, 26.1, 20.1 and 15.2 mW m^{-2} respectively [54]. These studies demonstrate that alterations in surface characteristics of anode materials can have significant effects on the performance of MiFCs.

This study focuses on improving the power densities of single-chamber MiFCs through surface alterations of stainless steel mesh anodes. There are a significant number of MiFC components which affect the performance of MiFCs (cathode, PEM, etc.), but the anode is primarily responsible for collecting the electrons from microorganisms and in that regard, may have more influence on the current generated in MiFCs than other non-biological components. The anode also comes into direct contact with microorganisms, which gives rise to an opportunity to improve electron transfer by the formation of a biofilm on the anode. Previous investigations as discussed in this literature review have set a precedent for the role of surface alterations in the improvement of MiFC performance [47, 54], and this study continues that line of research.

Table 2.1. Literature Summary of Single-Chamber Microbial Fuel Cells.

Source	Microorganism	Substrate	Reactor Type	Anode Material	Anode-Cathode Spacing	Power ($mW\ m^{-2}$)	Normalization	Power ($mW\ L^{-1}$)
[40]	Domestic Wastewater	Glucose (500 mg/L)	Batch	Carbon Cloth	2 cm	811	Cathode Projected Area	
					1 cm	432		
			Continuous Flow		1 cm	1540		51
[41]	Domestic Wastewater	Acetate (800 mg/L)	Batch	Carbon Paper	4 cm	506	Anode Projected Area	12.7
		Butyrate (1000 mg/L)				305		7.6
[42]	Domestic Wastewater	Acetate (1 g/L)	Batch	Carbon Paper	2 cm	1210	Anode Projected Area	
					4 cm	720		
[46]	Domestic Wastewater	Glucose (500 mg/L)	Batch	Carbon Cloth	4 cm	766	Anode Projected Area	
[44]	Domestic Wastewater	--	Continuous Flow	Graphite Rods	--	26	Total Anode Surface Area	
[39]	Domestic Wastewater	Glucose (1 g/L)	Batch	Carbon Cloth		480	Cathode Projected Area?	
[31]	Domestic Wastewater	Wastewater	Batch	Carbon Paper	4 cm	146 (no PEM)	Anode Projected Area	3.7
						28		0.1
		Glucose (600 mg/L)				381 (no PEM)		
						173		

3.0 EXPERIMENTAL PROCEDURES

3.1 MICROBIAL TECHNIQUES

Four main microbial cultures were used in testing the power generation of our MiFCs: a thermophilic, anaerobic sludge maintained in a reactor operated at Virginia Tech, a wastewater treatment plant (WWTP) sample of digester sludge placed directly in an iron-rich medium, a WWTP sample of digester sludge which was thickened and placed in the medium used during MiFC trials, and a WWTP sample of digester sludge which was thickened and placed in an iron-rich medium.

3.1.1 LABORATORY SLUDGE

The first type of anaerobic sludge in this study was maintained by a graduate student in the Department of Civil and Environmental Engineering at Virginia Tech. The reactor held thermophilically digested sludge (an approximate 50/50 mixture of primary and secondary sludge) kept at 55°C and was operated at a 12 day solids retention time (SRT). The inoculum was thickened waste activated sludge from a wastewater treatment plant (WWTP) in Duluth, Minnesota. Tap water was added to this sludge in the reactor to make a final solids content of 3%. 500 mg L^{-1} $FeCl_3$ as Fe was also added to the reactor to simulate conditions at the WWTP. The feed to the reactor was predigested in a thermophilic aerobic digester operated at 55°C and a 2.5 day SRT. This aerobic digester was aerated by injecting ambient air into the bottom of the reactor. This sludge was used in the first anaerobic experiment discussed in **Section 3.5**.

3.1.2 IRON-RICH SLUDGE

The second type of culture used in this study was a sample of digester sludge taken from Pepper's Ferry Wastewater Treatment Plant (PFWWTP) located in Radford, Virginia and maintained for four days in an anaerobic batch reactor. The sludge was mixed with an equal part of iron-rich (500 mg-Fe^{3+} L^{-1}) media listed in **Table 3.1**. The media was autoclaved, adjusted with 50% NaOH to a pH of 7 to 8, and then bubbled with 99.6 % nitrogen gas (Airgas, Inc.) for 15 minutes to displace any entrained oxygen. The sludge and media were then added to an Erlenmeyer flask with a rubber stopper, and placed inside an anaerobic glove box. The reactor was located on top of a heated stir-plate set at 30° C. The final sludge mixture was less dense than the other cultures used in this study. This sludge was used in the Sodium Azide Experiment discussed in **Section 3.5.3**.

Table 3.1. Iron-Rich Anaerobic Media Recipe.

Compound	g L^{-1}
Glucose	1.00
Yeast Extract	0.25
NH_4Cl	0.20
KCl	0.33
$CaCl_2 \cdot 2H_2O$	0.15
NaCl	0.30
$MgCl_2 \cdot 6H_20$	6.72
K_2HPO_4	1.26
KH_2PO_4	0.42
$FeCl_2 \cdot 4H_2O$	0.05
$FeCl_3$	1.45
$ZnCl_2$	0.00125
$MnCl_2 \cdot 4H_2O$	0.01250
$MoNa_2O_4 \cdot 2H_2O$	0.00191
$CoCl_2 \cdot 6H_2O$	0.00375
$NiCl_2 \cdot 6H_2O$	0.00250
$CuCl_2 \cdot 2H_2O$	0.00075
H_3BO_3	0.00125

3.1.3 LOW-IRON, 3% SLUDGE

The third type of culture used in this study was a sample of digester sludge taken from Pepper's Ferry Wastewater Treatment Plant (PFWWTP) and maintained for four days in an anaerobic batch reactor. The final solids content of the sludge was adjusted to 3% [57] through the following steps: 1. The solids content of the sludge was measured after being taken from the WWTP, 2. The sludge was centrifuged at 13,000 x g for 20 minutes, 3. The sludge was resuspended in the calculated amount of Nanopure water which, when mixed in a 1:1 ratio of media, would result in a final solids content of 3%. The media was similar to that used by He et al. [35] but was modified to contain 1000 mg L^{-1} glucose in place of sucrose (listed in **Table 3.2**) and was the same media as that used in the anaerobic MiFCs throughout this study. Similarly to iron-rich sludge, the media was autoclaved, adjusted with 50% NaOH to a pH in the range of 7 to 8, and then bubbled with 99.6 % nitrogen gas (Airgas, Inc.) for 15 minutes to displace entrained oxygen. The thickened sludge was then mixed with an equal part of media, poured into an Erlenmeyer flask with a rubber stopper and placed inside an anaerobic glove box. The reactor was located on top of a heated stir-plate set at 30° C. This sludge was used with iron enriched iron-rich, 3% sludge to test the effect of the sludge's media iron concentration on the power production in MiFCs (See **Section 3.5.4**).

Table 3.2. Anaerobic Media Recipe.

Compound	g L^{-1}
Glucose	1.00
Yeast Extract	0.25
NH_4Cl	0.20
KCl	0.33
$CaCl_2 \cdot 2H_2O$	0.15
NaCl	0.30
$MgCl_2 \cdot 6H_20$	6.72
K_2HPO_4	1.26
KH_2PO_4	0.42
$FeCl_2 \cdot 4H_2O$	0.05
$ZnCl_2$	0.00125
$MnCl_2 \cdot 4H_2O$	0.01250
$MoNa_2O_4 \cdot 2H_2O$	0.00191
$CoCl_2 \cdot 6H_2O$	0.00375
$NiCl_2 \cdot 6H_2O$	0.00250
$CuCl_2 \cdot 2H_2O$	0.00075
H_3BO_3	0.00125

3.1.4 IRON-RICH, 3% SLUDGE

The fourth type of culture used in this study was also a sample of digester sludge taken from Pepper's Ferry Wastewater Treatment Plant (PFWWTP) and maintained for four days in an anaerobic batch reactor. Similarly to low-iron, 3% sludge, the final solids content of the sludge was adjusted to 3% through the following steps: 1. The solids content of the sludge was measured after being taken from the WWTP, 2. The sludge was centrifuged at 13,000 x g for 20 minutes, 3. The sludge was resuspended in the calculated amount of Nanopure water which, when mixed in a 1:1 ratio of media, would result in a final solids content of 3%. The media for this sludge was the same iron-rich solution listed in **Table 3.1**. Similarly to iron-rich sludge and low-iron, 3% sludge, the media was autoclaved, adjusted with 50% NaOH to a pH in the range of 7 to 8, and then bubbled with 99.6 % nitrogen gas (Airgas, Inc.) for 15 minutes to displace

entrained oxygen. The thickened sludge was then mixed with an equal part of media, poured into an Erlenmeyer flask with a rubber stopper and placed inside an anaerobic glove box. The reactor was located on top of a heated stir-plate set at 30° C. This sludge was used to compare the effect of iron-enrichment on MiFC sludge in the experiment discussed in **Section 3.5.4** and in an experiment comparing the effect of anode type discussed in **Section 3.5.5**.

3.2 MICROBIAL FUEL CELL ASSEMBLY

The batch microbial fuel cells designed for this study were single chamber reactors with air-exposed cathodes, fabricated by the machine shop in the Department of Mechanical Engineering at Virginia Tech. **Figures 3.1, 3.2** and **3.3** below show the main components and assembly of a batch MiFC used in this work.

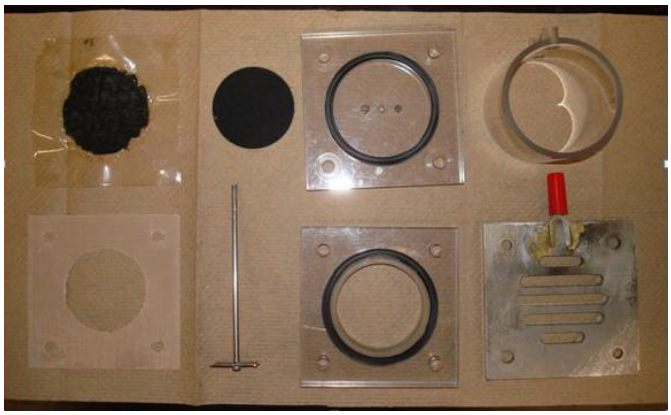

Figure 3.1 (L). Components of batch microbial fuel cell. Left to right, top to bottom: catalyst on membrane, diffusion layer, anode end plate, cell chamber, spacer, anode rod and anode, cathode end plate, collector plate.

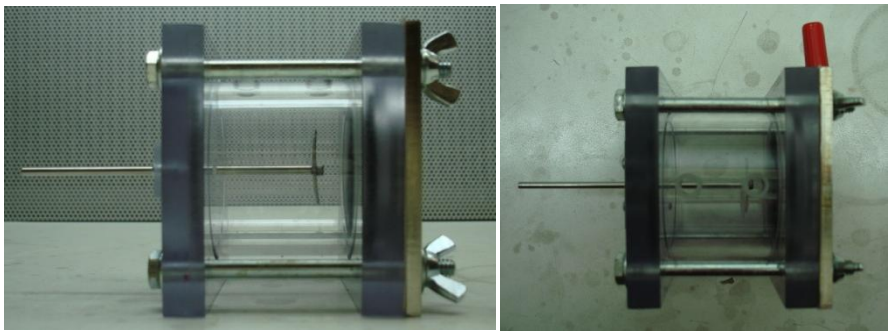

Figures 3.2 (L) and 3.3 (R). Side and overhead view of batch microbial fuel cell.

3.2.1 END PLATES/CHAMBER

The cathode and anode end plates of the batch MiFCs were constructed from Lexan® polycarbonate purchased from McMaster Carr Supply Company (Catalog No. 1749K64). They were machined with a hollow center through which the catalyst layer painted on the MEA was able to come into contact with oxygen in the surrounding air. The anode end plate contained a small hole through which the anode supporting rod was positioned.

The chambers, which housed the cultures, were constructed from hollow polycarbonate tubes obtained from McMaster Carr Supply Company (Catalog No. 8585K19). The batch chambers were 2.0 inches in length, with two injection ports drilled in the top of the chamber for sampling and the addition/removal of fluids.

3.2.2 MEMBRANE-ELECTRODE ASSEMBLY (MEA)

The cathode membrane-electrode assembly (MEA) was constructed by painting a 20 cm^2 catalyst layer comprised of carbon supported platinum catalyst with a loading of 0.4 mg-Pt cm^{-2} on one side of a 3.5 inch by 3.5 inch square of Nafion® 117. The recipe for the catalyst mixture is listed below in **Table 3.3**.

Table 3.3. MEA Catalyst Recipe.

Catalyst Ingredient	Amount
40 % Pt Catalyst (E-TEK 39.1% Pt on Vulcan XC-72)	0.02 g
Deionized (DI) Water	0.10 g
5 % Nafion Solution (DuPont™ DE521 Nafion® Solution)	0.17 g
Isopropyl Alcohol (IPA)	0.16 g

The constituents of the catalyst mixture were weighed then placed into a 1.5 mL conical centrifuge tube. The tube was then placed on an ultrasonic homogenizer (Model 300 V/T from BioLogics, Inc.) in order to completely blend the powdered catalyst with the liquid components. Once fully combined, the mixture was spread onto the Nafion® using a clean paintbrush in layers (i.e. first applying a vertical painted layer followed by a horizontal layer, etc.). The Nafion® was placed beneath a heated lamp on a vacuum plate heated to 60°C during the application of the catalyst layer to quicken the drying process.

3.2.3 ANODE

Three types of anodes were used in this work: carbon paper, stainless steel mesh (SSM) and stainless steel mesh coated with carbon nanostructures (CNSs). The carbon paper and the stainless steel mesh (purchased from the Goodfellow Corporation**)** were both used directly, while the CNS-enhanced anodes were manufactured via flame deposition on a stainless steel mesh substrate. The construction of these CNS-enhanced anodes was completed by members of the Multiphysics Research Group (MuRG) in the Department of Engineering Science and Mechanics at Virginia Tech.

Each CNS-enhanced anode was constructed by mounting a 6.5 cm^2 (or larger, to be cut to 25.4 mm x 25.4 mm) piece of stainless steel mesh in a clamp held 5.0 mm above the base of a nonpremixed ethylene/air flame (CNSs have been shown previously to form at heights between 4.0 and 10 mm above the flame base [58]). The flame was established over a co-flow Santoro burner using ethylene fuel (99.5% purity, Airgas, Inc., Part Number EY CP20) and air (Breathing Grade E Size 300 16PK CGA 346, Airgas, Inc., Part Number AI BCS3C058). The ethylene and air flow rates were 0.25 L min^{-1} (measured with an Omega FMA-1619A flow

meter) and 38 L min^{-1} (measured with an Omega FMA-1610A flow meter) respectively. Digital meters were affixed to the gas flow controllers.

A diagram and photo of the burner used to create these anodes are shown in **Figures 3.4** and **3.5**. The burner consisted of two concentric tubes: an inner tube of 11.1 mm inner diameter and an outer tube of 101.6 mm inner diameter, and maintained a flame temperature of approximately 1550°C. In order to stabilize the flame and make the flow velocity uniform, the burner was covered with ceramic honeycomb and the annulus of the burner contained glass beads.

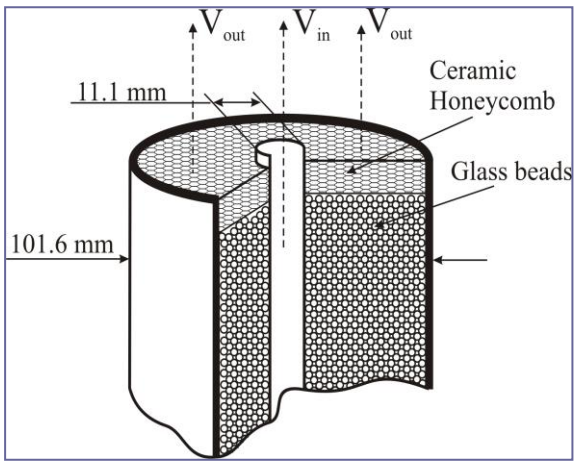

Figures 3.4 (L) and 3.5 (R). Diagram and image of co-flow burner with ethylene/air mixed flame. Reproduced with permission from [1].

3.3 IMPEDANCE TESTING

Impedance experiments on the batch fuel cells were performed in order to determine the significance of the various types of losses (e.g. activation, ohmic, diffusive) and to quantify the ohmic losses associated with the transport of electrons and ions within the MiFC [2]. Impedance is defined by Eq. 3.1 and 3.2 below, where Z= Impedance, V(t) = Time-dependant voltage,

i(t) = Time-dependant current, V_0, i_0 = Amplitudes, Z_0 = Impedance magnitude, ω = Frequency, and ϕ = Phase shift.

$$\boldsymbol{Z = \frac{V(t)}{i(t)}} \qquad \textbf{(3.1)}$$

Impedance is usually determined by observing a system's response to a sinusoidal current perturbation so that:

$$\boldsymbol{Z = \frac{V_0 \cos(\omega t + \emptyset)}{i_0 \cos(\omega t)} = \frac{V_0 e^{\sqrt{-1}(\omega t + \emptyset)}}{i_0 e^{\sqrt{-1}\omega t}} = Z_0(\cos \emptyset + \sqrt{-1} \sin \emptyset)} \qquad \textbf{(3.2)}$$

Therefore, the impedance can be separated into a real and imaginary component:

$$\boldsymbol{Z_{real} = Z_0 \cos \emptyset} \qquad \textbf{(3.3)}$$

$$\boldsymbol{Z_{imag} = Z_0 \sqrt{-1} \sin \emptyset} \qquad \textbf{(3.4)}$$

The ohmic impedance of a fuel cell is modeled as a simple resistor for which the ohmic impedance (Z_{ohm}) is equal to the ohmic resistance (R_{ohm}), the change in impedance with respect to frequency is zero, and the imaginary impedance (Z_{imag}) is zero.

$$\boldsymbol{Z_{ohm} = R_{ohm}} \qquad \textbf{(3.5)}$$

$$\boldsymbol{\frac{\partial Z_{ohm}}{\partial \omega} = 0} \qquad \textbf{(3.6)}$$

$$\boldsymbol{Z_{imag} = 0} \qquad \textbf{(3.7)}$$

In a normal PEMFC fuel cell, the losses can be represented graphically in a Nyquist plot (**Figure 3.6**). As the input frequency increases (from right to left in the plot), information about the relative magnitude of ohmic losses, anode activation losses and cathode activation losses in

the fuel cell can be inferred from the plot. In **Eq. 3.5**, **Eq. 3.7** and the Nyquist plot, we see that when Z_{imag} is equal to zero at the highest frequency, the corresponding value of Z_{real} is equal to the ohmic loss of the fuel cell. The ohmic losses of our MiFCs were ascertained by determining this value from of a similar, experimentally generated Nyquist plot.

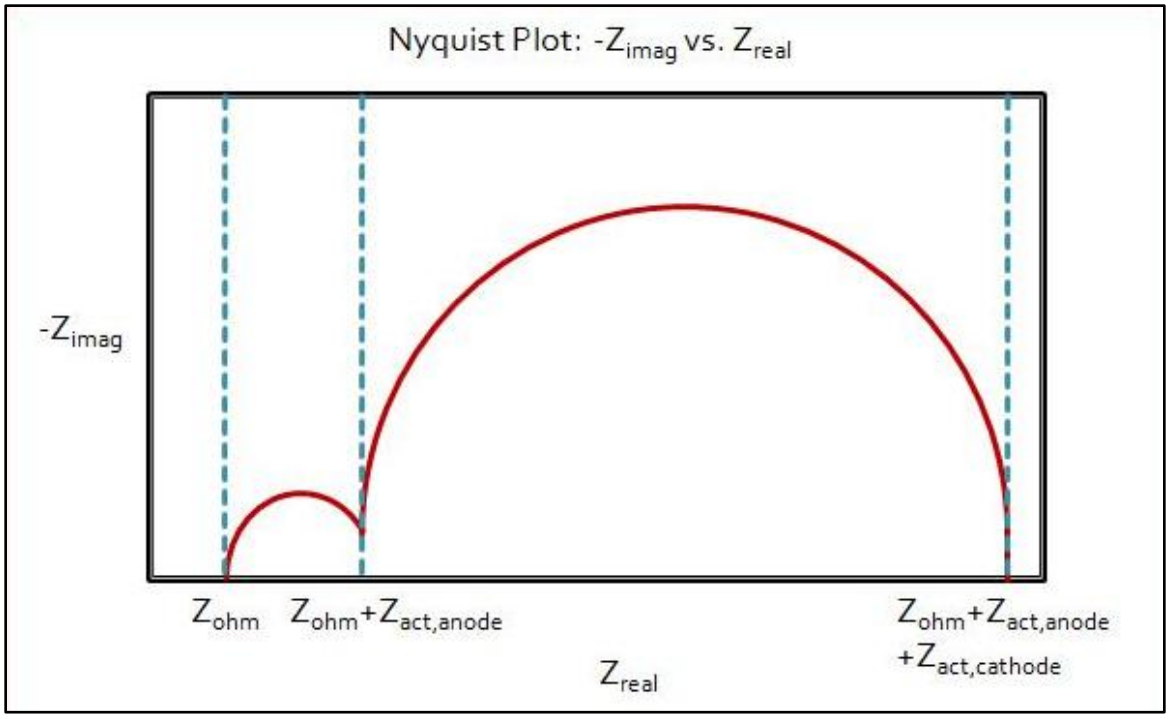

Figure 3.6. Nyquist plot of a hypothetical fuel cell.

The internal resistances of the six MiFCs used in this work (four batch MiFCs and two continuous-flow MiFCs converted for batch use) were compared after their use in the Low-Iron, 3% Sludge Experiment (see **Section 3.5.6**). Three MiFCs were assembled with stainless steel mesh anodes (6.5 cm^2) positioned 2.0 cm from the cathode and three were assembled with CNS-enhanced anodes (6.5 cm^2) positioned 2.0 cm from the cathode. All six fuel cells were filled with anaerobic sludge media (**Table 3.2**), inoculated with the low Fe, 3% sludge, connected to a potentiostat and tested for their power generation. At the end of the experiment, the impedance

test was conducted while microorganisms were still present on the anodes of the MiFCs. Using ZPlot, the test was conducted by passing 1.0 mA of alternating current through each MiFC at frequencies ranging from 100,000 to 0.01 Hertz. The overall cell resistance was determined based on the high frequency impedance. This test was used to monitor the performance degradation of the cathode and other cell components.

A similar impedance test was run on the four original batch MiFCs (two with uncoated stainless steel mesh anodes and two with CNS-coated anodes) using sterile (low Fe) anaerobic sludge media (**Table 3.2**) in order to compare the results with those from the impedance test conducted in the presence of microorganisms.

3.4 ABIOTIC MEA TESTING

In order to check the performance of the MEAs, some of the MiFCs used in this study were periodically tested without the addition of microorganisms. The abiotic test consisted of filling the MiFC with dilute sulfuric acid (0.5-1.0 M) and placing a small gas sparger (Aquarium Pharmaceuticals Rena® 2 inch micro-bubbler) in the chamber directly underneath the anode (see **Figure 3.8**).

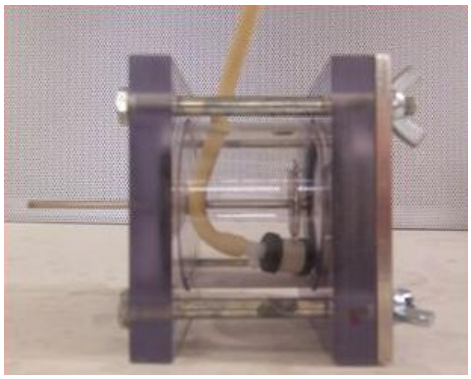

Figure 3.8. Abiotic MiFC setup.

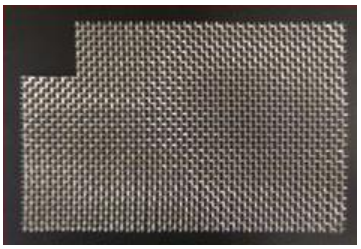

Figure 3.9. Pt coated Nb mesh.

The sparger was manually cut down to approximately 1.5 cm in length. A 6.5 cm^2 (1.0 in^2) square piece of platinum coated niobium mesh (Anomet Products, platinum clad mesh anode) was used as the anode in these tests (**Figure 3.9**). A small piece of tubing was attached to the gas sparger and run through one of the sampling ports on the MiFC chamber. This tubing was connected to a fuel cell test stand and 50ccm-100ccm hydrogen

gas was flowed through the line and sparger. A second portion of tubing was connected to the second MiFC sampling port and used to vent hydrogen gas to the ambient environment. The MiFC was then electrically connected to the potentiostat (Solartron 1480 MultiStat) and a potentiodynamic experiment was run using Corrware software which generated a polarization curve (current-voltage curve) for the fuel cell. The potentiodynamic experiment swept from the open circuit voltage of the fuel cell (OCV) down to 0.01-0.1 volts.

3.5 BATCH ANAEROBIC SLUDGE FUEL CELL TESTING

Five sets of batch experiments were conducted in this study to determine the power production of biomass using CNS-enhanced anodes:

1. A pseudo-sterile experiment to quantify power generation from the media used in the rest of the biotic experiments (two trials; four MiFCs were tested: two replicates containing CNS-enhanced anodes and two replicates containing uncoated stainless steel mesh anodes).
2. An anaerobic experiment using the sludge discussed in **Section 3.1.1** (two trials; four MiFCs were tested: two replicates containing CNS-enhanced anodes and two replicates containing uncoated stainless steel mesh anodes).
3. A sodium azide experiment using the anaerobic sludge discussed in **Section 3.1.2** to prove that the power generation from batch experiments was from microbial activity (one trial; four MiFCs were tested, all containing CNS-enhanced anodes).
4. An anaerobic experiment to test the effect of biomass acclimation to iron-rich conditions on the subsequent power generation using sludges discussed in **Sections 3.1.3** and **3.1.4** (one trial; six MiFCs were tested, all containing CNS-enhanced anodes).

5. An anaerobic experiment using the sludge discussed in **Section 3.1.3** (one trial; six MiFCs were tested: three replicates containing CNS-enhanced anodes and three replicates containing uncoated stainless steel mesh anodes).

Certain preparatory procedures were followed for each of the experiments in this study. The fuel cell components and media (**Table 3.2**) were kept as sterile as possible before inoculation by assembling the MiFCs in a sterile laminar flow hood, wiping the cell components (except the MEA) liberally with 75% ethanol (by volume) and autoclaving the media for 30 minutes at 121° C. Prior to introduction into the MIFC chamber, the media was bubbled for 20 minutes with 99.6% nitrogen gas (Airgas, Inc.) to strip dissolved oxygen.

In all of the experiments in the pseudo-sterile and anaerobic studies, the MiFCs were placed on a multistir plate and continuously mixed for the duration of the test. During each anaerobic experiment, a Tedlar bag (evacuated using a vacuum pump) was placed on one sampling port of each MiFC to capture any gases generated by the microorganisms when under positive pressure. The fuel cells were allowed to equilibrate for approximately 20 minutes. The open circuit voltage (OCV) was measured and a polarization curve was generated for each MiFC by running a potentiodynamic test consisting of a voltage sweep from the OCV to a voltage equal to or less than 0.1 V. After preliminary polarization curves were recorded, potentiostatic tests were conducted at approximately one-half the average OCV of the MiFCs. The performance of each MiFC in this study was determined using a Solartron 1480 MultiStat with Corrware software. Current densities and power densities were calculated based on the projected surface area of the anode (6.5 cm^2).

In all tests except the Pseudo-Sterile Experiment (**Section 3.5.1**) and the first trial of the Laboratory Sludge Experiment (**Section 3.5.2**), the glucose level and pH were monitored daily. Glucose samples were extracted through the sampling ports on the MiFCs using a syringe and filtered through a 0.45 μm nitrocellulose membrane before being analyzed according to the procedure listed in **Section 3.5.6** [57]. Glucose was added to the fuel cells when the concentration fell below 100 mg L^{-1} to achieve a maximum concentration of 500 mg L^{-1}, and the pH was adjusted to be within the range of 7.0 to 8.5.

3.5.1 PSEUDO-STERILE TESTING PREPARATION

In order to establish that any current generated by the MiFCs was due to the presence of microorganisms, two pseudo-sterile trials were run in duplicate and on two separate occasions using the media listed in **Table 3.2**. In each of the two trials, four MiFCs were tested (two with 6.5 cm^2 CNS-coated anodes and two with 6.5 cm^2 plain stainless steel mesh anodes) at an anode-cathode spacing of 2.0 cm using the media in **Table 3.2**. The pseudo-sterile techniques discussed in **Section 3.5** limited the initial concentration of microorganisms but were not sufficient to keep the MiFCs completely abiotic. However, the techniques were sufficient to limit the microbial density to a small fraction of the density used during the biotic anaerobic experiments.

3.5.2 LABORATORY SLUDGE TESTING PREPARATION

After completing the Pseudo-Sterile Experiment, the first anaerobic experiment was conducted through two separate trials, each comparing the power production using CNS-

enhanced and plain stainless steel anodes (each anode assembly was run in duplicate during each trial). The anodes were all 6.5 cm^2 and were set at a distance of 2.0 cm from the cathode.

The biomass used in the experiment was laboratory sludge, discussed in **Section 3.1.1**. A 10 mL sample of biomass was added to each cell before filling the rest of the volume with media. In the case that any oxygen was trapped during transfer from the parent digester, the biomass was deoxygenated using a vacuum flask and pump for ten minutes before its addition to the MiFCs. The glucose level and pH were monitored daily only during the second of the two anaerobic trials.

3.5.3 SODIUM AZIDE TESTING PREPARATION

After running the first set of experiments, it was important to determine whether the observed power production in the MiFCs could be entirely attributed to microbial activity. To accomplish this, an experiment was run using iron-rich sludge (discussed in **Section 3.1.2**), during which half of the MiFCs were dosed with a microbial toxin in an attempt to kill the power-producing microorganisms. A drop in the power production corresponding to the addition of the toxin would show that the power could be attributed to microorganisms.

Four MiFCs were tested with CNS-coated anodes (6.5 cm^2) at an anode-cathode spacing of 2.0 cm using the media in **Table 3.2**. To fill the MiFCs, a 10 mL sample of biomass (iron-rich sludge) was first added to each cell before filling the rest of the volume with media. Once all four of the fuel cells began to produce power, 10 mM of sodium azide (NaN_3) was added to two of the cells with a syringe through a sampling port in order to kill the microorganisms.

3.5.4 IRON-RICH VS. CONTROL MEDIA TESTING PREPARATION

After generating power using laboratory sludge and iron-rich sludge which had been acclimated in iron-rich media, an experiment was conducted to ascertain whether the addition of iron to the microorganisms before placement in MiFCs was necessary for power production. This experiment used low-iron, 3% and iron-rich, 3% sludges, which had been acclimated in the normal MiFC media and the MiFC with an additional 500 mg-Fe^{3+} L^{-1} respectively.

Six MiFCs were tested with CNS-coated anodes (6.5 cm^2) at an anode-cathode spacing of 2.0 cm. Three MiFCs were filled with a 10 mL sample of low-iron, 3% sludge, while the remaining three MiFCs were filled with a 10 mL sample of iron-rich, 3% sludge. The remaining volume of each of the six cells was then filled with media.

3.5.5 LOW-IRON, 3% SLUDGE TESTING PREPARATION

Another anaerobic experiment was conducted comparing the power production using CNS-enhanced and plain stainless steel anodes (each anode assembly was run in triplicate). The anodes were all 6.5 cm^2 and were set at a distance of 2.0 cm from the cathode. All six MiFCs were filled with a 10 mL sample of iron-rich, 3% sludge and remaining volume of each cell was then filled with media (**Table 3.2**). This test was used as a third trial (in conjunction with the two trials discussed in **Section 3.5.2**) to test the hypothesis that CNSs enhance power production in MiFCs.

3.5.6 GLUCOSE MONITORING

The glucose samples taken from the batch anaerobic experiments were analyzed according to the following procedures [57]:

1. The samples were filtered through a 0.45 μm filter.
2. 100 μL of each filtered sample was placed into a 1.5 mL centrifuge tube.
3. To each sample, the following was added in order:
    a. 100 μL of 5% phenol solution
    b. 500 μL of concentrated sulfuric acid
4. Each sample was mixed using a vortexer after the addition of each solution.
5. The color was allowed to develop in the dark for at least 10 minutes.
6. 200 μL of each sample was placed in a microplate.
7. The microplate was placed in a spectrophotometer.
8. The absorbance for each sample was read at a wavelength of 490 nm.
9. The results were compared against a standard curve to determine the glucose concentration.

The results of glucose concentration monitoring during batch experiments are included in **Appendix A**.

4.0 NUMERICAL SIMULATION

In the literature to date, little progress has been made in attempting to match the results of numerical models of MiFC to empirical data gleaned from laboratory experiments. In fact, the field is still highly experimental, with only a few studies concentrating fully on model predictions of power generation from MiFCs. As part of this thesis, an attempt was made to use a biofilm modeling approach developed by Marcus et al. [4] to match the successful power production from the batch MiFCs used in the aforementioned experiments.

4.1 DEVELOPMENT

The approach taken by Marcus et al. is to model the anode of a MiFC as a "biofilm anode" which consist of microorganisms in a solid, conductive matrix. The microorganisms oxidize an electron donor, providing electrons which are conducted through this matrix (with a characteristic conductivity, k_{bio}) to the anode. The model is one-dimensional and uses the Nernst equation, a Monod expression for microbial kinetics and Ohm's law to determine the current density on the MiFC anode. A summary of these equations, as well the others used in the model, is given below.

Rate of Electron Donor (ED) Utilization:

$$q = q_{max}\, \emptyset_a \left(\frac{S_d}{K_{S_d}+S_d}\right)\left(\frac{1}{1+exp\left[-\frac{F}{RT}\eta\right]}\right) \qquad \textbf{(4.1)}$$

Definitions:

q specific rate of ED utilization (mmol-ED mg-VSS^{-1} day^{-1})

S_d ED concentration (mmol-ED cm^{-3})
η local potential (V)
K_{S_d} half-max-rate ED concentration (mmol-ED cm^{-3})
$\emptyset_a$ volumetric fraction of active biomass (dimensionless)
q_{max} maximum specific rate of ED utilization (mmol-ED mg-VSS^{-1} day^{-1})
F Faraday's constant (96485 C mol e^{-1})

The equation for the rate of electron donor utilization is derived for a soluble electron donor (e.g. acetate or glucose) and solid-state electron acceptor (the anode). It is described by a dual donor-acceptor Monod model [59] where Monod kinetics for the electron donor is reflected in the first term of the equation and by the Nernst equation which is reflected in the second term for the electron acceptor. For a quasi-steady state of biomass, the variables q, S_d, η, and $\emptyset_a$ are dependent on space only. As will be discussed in the results (**Chapter 5.0**) the parameter q_{max} was altered to fit experimental data.

Rate of Endogenous Respiration:

$$r_{res} = b_{res}\emptyset_a\left(\frac{1}{1+exp\left[-\frac{F}{RT}\eta\right]}\right) \quad \textbf{(4.2)}$$

Definitions:

r_{res} specific rate of endogenous respiration (day^{-1})
b_{res} endogenous decay coefficient for active biomass (day^{-1})

Endogenous respiration occurs when microorganisms oxidize active biomass for use in cellular maintenance functions. This results in an increased rate of production of inert biomass. The rate of endogenous respiration is based on the endogenous decay coefficient (b_{res}), the fraction of active biomass ($\emptyset_a$) and the local potential (η).

Electron Donor Mass Balance:

$$0 = D_{ED,f} \frac{\partial^2 S_d}{\partial x^2} - X_{f,a} q \quad \textbf{(4.3)}$$

The electron donor mass balance equation is based on steady-state utilization (q) of electron donor (S_d) in and diffusion through the biofilm. The boundary conditions include a zero mass flux condition at the interface between the biofilm and anode (**Eq. 4.4**) and a convective flux from the bulk liquid to the interface between biofilm surface and the bulk liquid (**Eq. 4.5**). The convective coefficient at the boundary is based on the diffusivity of the bulk liquid ($D_{ED,l}$) and the diffusion layer thickness (L). The product of this convective coefficient and the ED concentration difference (bulk liquid to biofilm surface) is equated to the ED diffusion through the biofilm.

Boundary Conditions:

$$0 = D_{ED,f} \frac{\partial S_d}{\partial x}|_{x=0} \quad \textbf{(4.4)}$$

$$D_{ED,l} \frac{\partial S_d}{\partial x}|_{x=L_f} = D_{ED,f} \frac{\partial S_d}{\partial x}|_{x=L_f} = \left(\frac{D_{ED,l}}{L}\right)(S_{d,bulk} - S_{d,surface}) \quad \textbf{(4.5)}$$

Definitions:

$D_{ED,f}$	diffusion constant for ED in the biofilm (cm^2 day^{-1})
$D_{ED,l}$	diffusion coefficient for ED in the bulk liquid (cm^2 day^{-1})
$X_{f,a}$	density of active biomass (mg-VSS cm^{-3})
$S_{d,bulk}$	ED concentration in the bulk liquid (mmol-ED cm^{-3}),
$S_{d,surface}$	ED concentration at the biofilm surface (mmol-ED cm^{-3}).
L	thickness of the diffusion layer (cm)

Electron Balance & Ohm's Law:

$$0 = \kappa_{bio} \frac{\partial^2 \eta}{\partial x^2} - \frac{F\gamma_1}{\tau} f e^0 X_{f,a} q - \frac{F\gamma_2}{\tau} X_{f,a} r_{res} \quad \textbf{(4.6)}$$

The electron balance equation takes into account Ohm's law (first term) modeling the biofilm as a porous conductor with a conductivity of κ_{bio}, the generation of electrons through the oxidation of the electron donor (second term) using the donor's electron equivalence (γ_1) and the generation of electrons through endogenous respiration (third term) using the electron equivalence of active biomass (γ_2). The boundary conditions for this equation include a defined voltage at the anode (V_{anode}) and a zero-flux condition at the biofilm-bulk liquid interface.

Boundary Conditions:

$$\eta|_{x=0} = V_{anode} \quad \textbf{(4.7)}$$

$$\frac{\partial \eta}{\partial x}|_{x=L_f} = \frac{j|_{x=L_f}}{\kappa_{bio}} = 0 \quad \textbf{(4.8)}$$

Definitions:

κ_{bio}	biofilm conductivity mS cm^{-1}
j	current density (mA cm^{-2})
γ_1	electron equivalence of ED (mmol-e^- mmol-ED^{-1})
γ_2	electron equivalence of active biomass (mmol-e^- mmol-ED^{-1}) based on an empirical formula for microbial cells, CnHaNbOc; Rittmann and McCarty, 2001)
τ	time conversion (86,400 s day^{-1})
fe^0	fraction of electrons from the ED used for energy generation to support synthesis (dimensionless)
V_{anode}	anode voltage (V)

<u>Biomass Balance:</u>

$$1 = \emptyset_a + \emptyset_i \quad \textbf{(4.9)}$$

$$\frac{\partial \emptyset_a}{\partial t} + \frac{\partial (v\emptyset_a)}{\partial x} = Yq - r_{res} - r_{ina} \quad \textbf{(4.10)}$$

$$\frac{\partial \emptyset_i}{\partial t} + \frac{\partial (v\emptyset_i)}{\partial x} = \frac{X_{f,a}}{X_{f,i}} r_{ina} \quad \textbf{(4.11)}$$

$$r_{ina} = b_{ina}\emptyset_a \quad \textbf{(4.12)}$$

$$\frac{\partial v}{\partial x} = \mu_a + \mu_i \quad \textbf{(4.13)}$$

$$v(t,x') = \int_0^{x'} (\mu_a + \mu_i) dx \quad \textbf{(4.14)}$$

$$\frac{\partial \emptyset_a}{\partial t} + \frac{\partial (v\emptyset_a)}{\partial x} \equiv \mu_a \quad \textbf{(4.15)}$$

$$\frac{\partial \emptyset_i}{\partial t} + \frac{\partial (v\emptyset_i)}{\partial x} \equiv \mu_i \quad \textbf{(4.16)}$$

$$\frac{dL_f}{dt} = v(t, L_f) - b_{det} L_f \quad \textbf{(4.17)}$$

The conservation equation (**Eq. 4.9**) states that the volumetric fractions of active ($\emptyset_a$) and inactive ($\emptyset_i$) biomass always sum to one. The mass balance for active biomass (**Eq. 10**) equates the accumulation (first term on left) and advection (second term on left) with the growth of active biomass (first term on right) less that used for endogenous respiration (second term on right) and inactivation/decay (third term on right). The mass balance for inactive biomass (**Eq. 11**) equates the accumulation and advection of inert biomass in the biofilm to the rate of inactivation of active biomass (r_{ina}). **Eq. 4.17** describes the change in biofilm thickness (L_f) with time based on the advective velocity of the biofilm matrix (v) and the detachment rate of biomass from the biofilm surface (b_{det}). The advective velocity of the matrix is calculated from the accumulation and advection of active and inactive biomass (i.e. **Eqs. 4.10** and **4.11**).

Definitions:

$\emptyset_i$	volumetric fraction of inert biomass (dimensionless)
Y	true yield (mg-VS mmol-ED^{-1})
$X_{f,i}$	density of inert biomass (mg-VS cm^{-3})
L_f	biofilm thickness (cm)
v	advection velocity of the biofilm matrix (cm-day^{-1})
μ_a	net specific growth rate for active biomass (day^{-1})
μ_i	net specific growth rate for inert biomass (day^{-1})
r_{ina}	rate of inactivation of biomass (day^{-1})
b_{ina}	first-order inactivation rate coefficient (day^{-1})
b_{det}	first-order rate coefficient of biomass loss due to detachment (day^{-1})

4.2 ALTERATIONS

The Marcus model, as published, is based on acetate as an electron donor, *Geobacter sulfurreducens* as the main biocatalyst and a constant concentration of substrate in the bulk liquid. The following alterations were made to the model in order to better fit the microorganisms and substrate use in the aforementioned batch MiFC experiments.

1. Glucose instead of acetate was used as the electron donor.
2. Average biokinetic parameters for anaerobic sludge were used in the place of parameters based on *Geobacter sulfurreducens*.
3. The bulk liquid concentration was based on actual measurements of glucose concentration made during batch experiments.
4. The anode potential (V_{anode}) was calculated from fed-batch experiments using an Ag/AgCl reference electrode.

4.3 SOLUTION APPROACH

Using Mathematica® software (Wolfram Research, Inc.), the following strategy was employed in solving the system of equations presented as **Eqs. 4.1-4.17**:

1. Discretize the system of quasi-steady, one dimensional equations given by **Eqs. 4.3 – 4.8** using a centered difference approximation.
2. Solve the resulting system of nonlinear equations (**Eqs. 4.3-4.8**) using Newton's method [60] and a discretized Jacobian matrix to obtain a steady-state solution for the local potential (η) and electron donor concentration (S_d) at the current time step.

3. Solve **Eqs. 4.9-4.14** based on results from the quasi-steady solution and the values of $ø_a$ and $ø_i$ from the current time step for the advective velocity (v) of the biofilm.
4. Discretize and solve **Eqs. 4.15** and **4.16** using an implicit Euler method [60] and matrix methods with a time step of 0.001 days, generating values of $ø_a$ and $ø_i$ (the fractions of active and inactive biomass) for the next time step (t+1) in the biofilm. The use of an implicit method requires iterating over Steps 1-3 and **Eqs. 4.15** and **4.16** in the routine to determine values for ED concentration (S_d), local potential (η) and advective velocity (v) at the next time step (t+1).
5. Update the biofilm thickness (L_f) by discretizing and solving **Eq. 4.17** using a backward difference approximation and iterating to a steady-state value.
6. Partition the new biofilm into 50 segments (i.e. $\Delta x = L_f/50$) and return to Step 1.

5.0 EXPERIMENTAL AND NUMERICAL MODELING RESULTS

The results from the experiments conducted in this study as well as the computational modeling are discussed in the following sections. All current and power densities are based on the projected surface area of the anode. The maximum current and power densities determined from potentiostatic tests were calculated after the initial current density spike (generally lasting for the first 10-15 hours of testing) which was believed to be caused by electrochemical effects.

5.1 IMPEDANCE TESTING RESULTS

Two impedance tests were conducted on the batch MiFCs used in this study – one which determined the resistance of the four original batch MiFCs with sterile anaerobic media and one which determined the resistance of the four original batch MiFCs and the two batch-converted, continuous-flow MiFCs after a biotic experiment (the Low-Iron, 3% Sludge Experiment). The results generated using ZPlot software with a frequency range of 0.01 to 100000 Hz and an anode-cathode spacing of 2.0 cm are summarized in **Table 5.1** below.

Table 5.1. Batch MiFC Impedance Testing Results.

Trial	Anode Type[a,b]	Cell No.	Ohmic Resistance (Ω)	Anode Type[a,b]	Cell No.	Ohmic Resistance (Ω)
1 (Biotic)	CNS	1	17	SSM	2	10
		3	18		4	12
		5	15		6	12
2 (Abiotic)	CNS	1	19	SSM	3	26
		2	17		4	18

[a] SSM = uncoated stainless steel mesh anode; [b] CNS = carbon nanostructure-coated stainless steel mesh anode

The Nyquist plots from the impedance tests are given below in **Figure 5.1** (with microbial growth) and **Figure 5.2** (with sterile media).

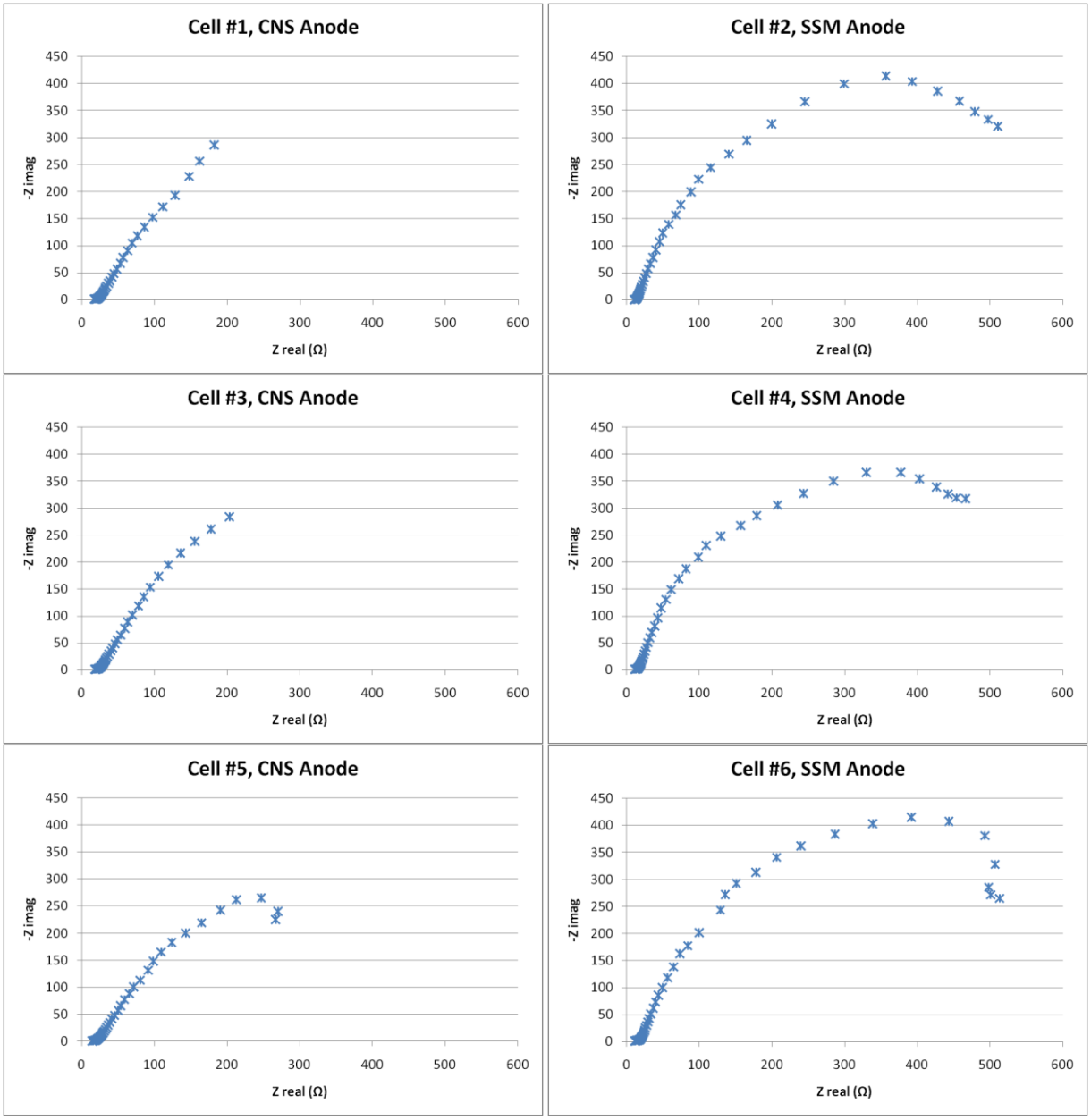

Figure 5.1. Nyquist plots from impedance tests on MiFCs with microbial growth.

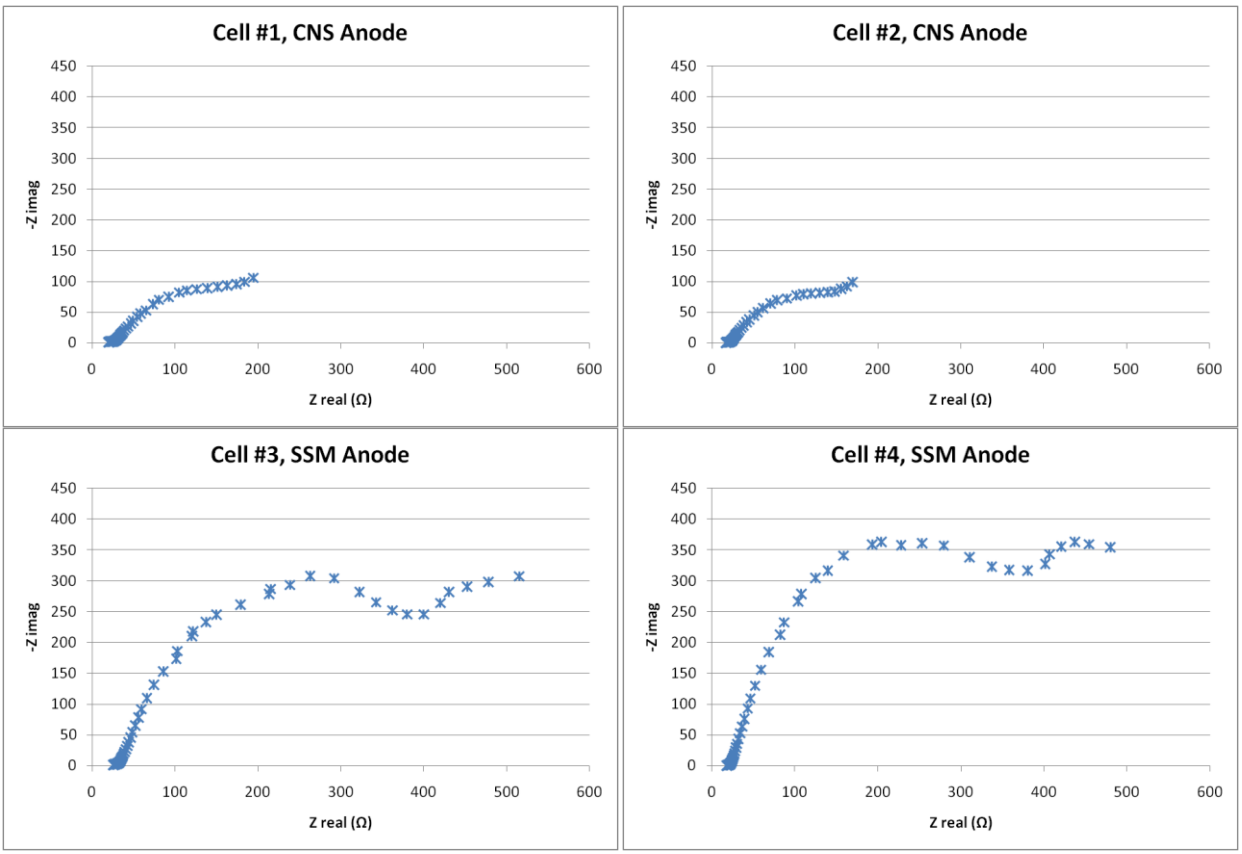

Figure 5.2. Nyquist plots from impedance tests on MiFCs with sterile anaerobic media.

From the Nyquist plots, the ohmic resistances of the MiFCs were determined by the leftmost intercept of the semicircle on the Z_{real} axis (see **Section 3.3**).

With microbial growth in the fuel cell and on the anode, the MiFCs with CNS-coated anodes had larger ohmic resistances than those with plain anodes. This may be due to a thicker biofilm on the CNS-coated anodes which impeded electronic and ionic transport to and from the anode surface. This hypothesis is reinforced by the fact that the ohmic resistances of the MiFCs were more similar when sterile media when no microbial growth was present, than after the biotic experiment.

5.2 PSEUDO-STERILE MIFC TESTING RESULTS

A summary of the results of potentiostatic pseudo-sterile tests conducted with anaerobic sludge media are given below in **Table 5.2**.

Table 5.2. Summary of Pseudo-Sterile Testing Results.

Trial	Anode Type[a,b]	Cell No.	Voltage (V)	Maximum Current (mA m^{-2})	Maximum Power (mW m^{-2})
1	SSM	3	0.15	3.65	0.548
		4	0.15	1.08	0.163
	CNS	1	0.15	222	32.2
		2	0.15	205	30.8
2	SSM	2	0.20	13.1	2.61
		3	0.20	1.57	0.314
	CNS	1	0.20	38.0	7.59
		4	0.20	33.8	6.76

[a] SSM = uncoated stainless steel mesh anode; [b] CNS = carbon nanostructure-coated stainless steel mesh anode

The largest power density obtained from the MiFCs using the 1000 mg-glucose L^{-1} media was 32.2 mW m^{-2}, obtained by a MiFC with a CNS-coated anode in the first trial of the experiment. It is interesting to note that even without purposefully inoculating the fuel cells with microorganisms, the MiFCs with CNS-coated anodes outperformed their uncoated (plain stainless steel mesh) counterparts. This indicated that perhaps the sterile techniques employed in this experiment were not enough to completely alleviate the effect of microbial activity on power production in the MiFCs. However, subsequent results from biotic experiments show that this power generation is low in comparison with inoculated MiFCs.

Figures 5.3 and **5.4** show polarization curves generated immediately preceding the potentiostatic tests of Trial 1 and Trial 2 respectively. These figures show that the MiFCs with CNS-coated anodes performed better even with a small microbial population.

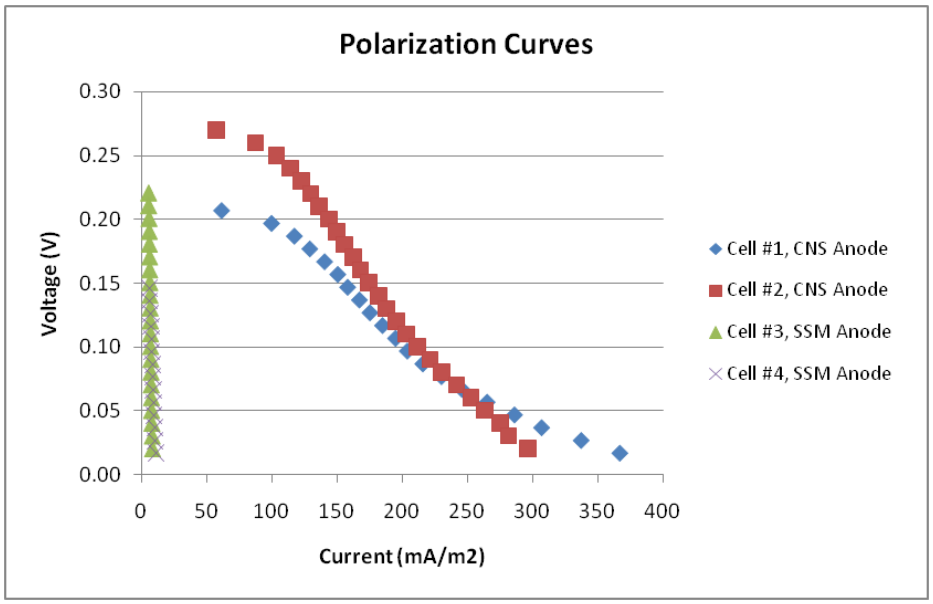

Figure 5.3. Polarization curves from all MiFCs tested during Trial 1 of the Pseudo-Sterile Experiment.

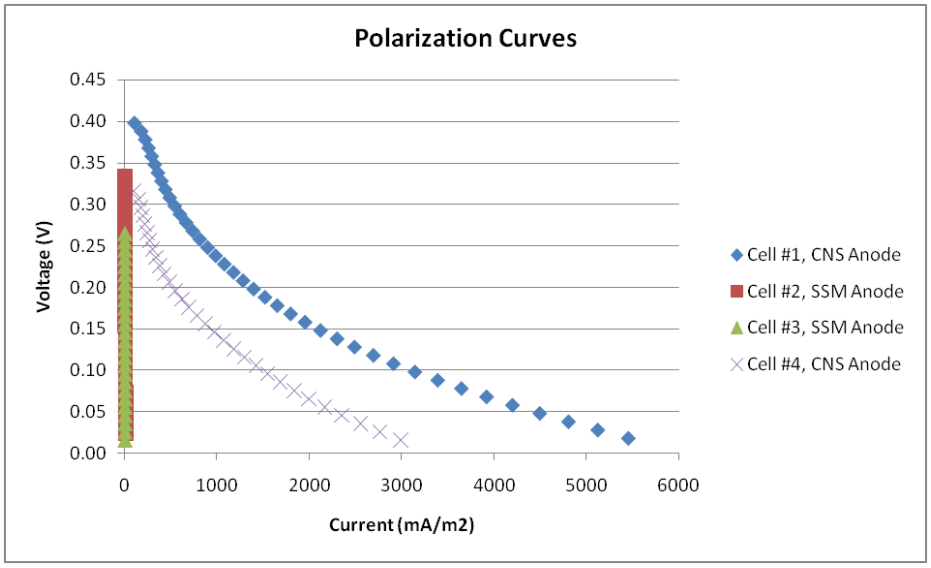

Figure 5.4. Polarization curves from all MiFCs tested during Trial 2 of the Pseudo-Sterile Experiment.

The differences in the polarization curves of MiFCs with CNS-coated versus uncoated anodes can be explained by the hypothetical polarization curve below. The larger anodic losses of MiFCs with uncoated anodes are manifested in the polarization curves as a much steeper drop in the voltage with current. The polarization curves also reinforce the theory that the activation overpotential due to reaction kinetics at the anode dominates the losses of the MiFCs used in this study. **Figure 5.5** below shows how losses are represented in polarization curves.

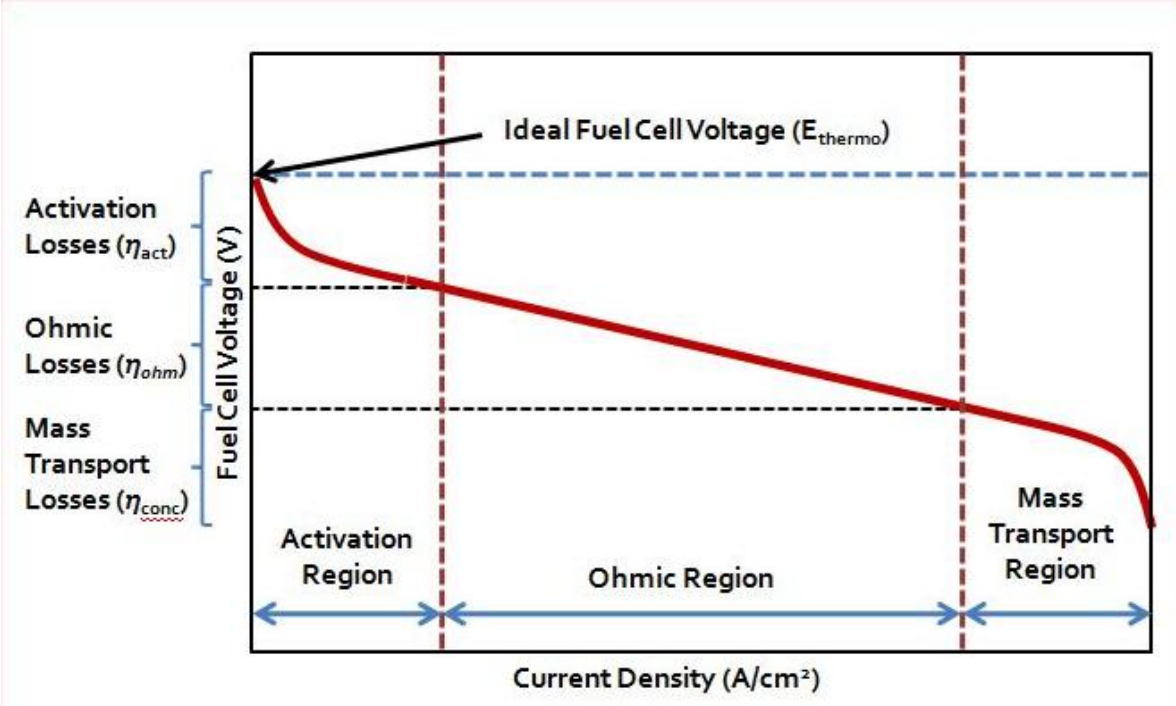

Figure 5.5. A hypothetical polarization curve.

When comparing the hypothetical polarization curve in **Figure 5.5** to **Figures 5.3** and **5.4**, one can see that the MiFCs are dominated by activation losses caused by slow reaction kinetics at the electrode. A small ohmic region is discernable in the curves, but there are almost no visible losses attributable to mass transport (the transport of reaction products away from an electrode). Similar results are seen in the polarization curves taken at the beginning of subsequent experiments.

Figures 5.6 and **5.7** show the potentiostatic results from Trial 1 and Trial 2 respectively. All MiFCs were tested for 65 hours. The MiFCs with CNS-coated anodes generate a characteristic curve in which electrochemical effects cause an initial spike in the current density, which then declines to a baseline value close to zero. As the microorganisms grow and begin interacting with the anode, the current density increases to a maximum value. The current density then declines as the growth of the microorganisms slows. This trend is easily seen in Cells #1 and #2 from Trial #2 and to a lesser extent in Cells #1 and #4 from Trial #2.

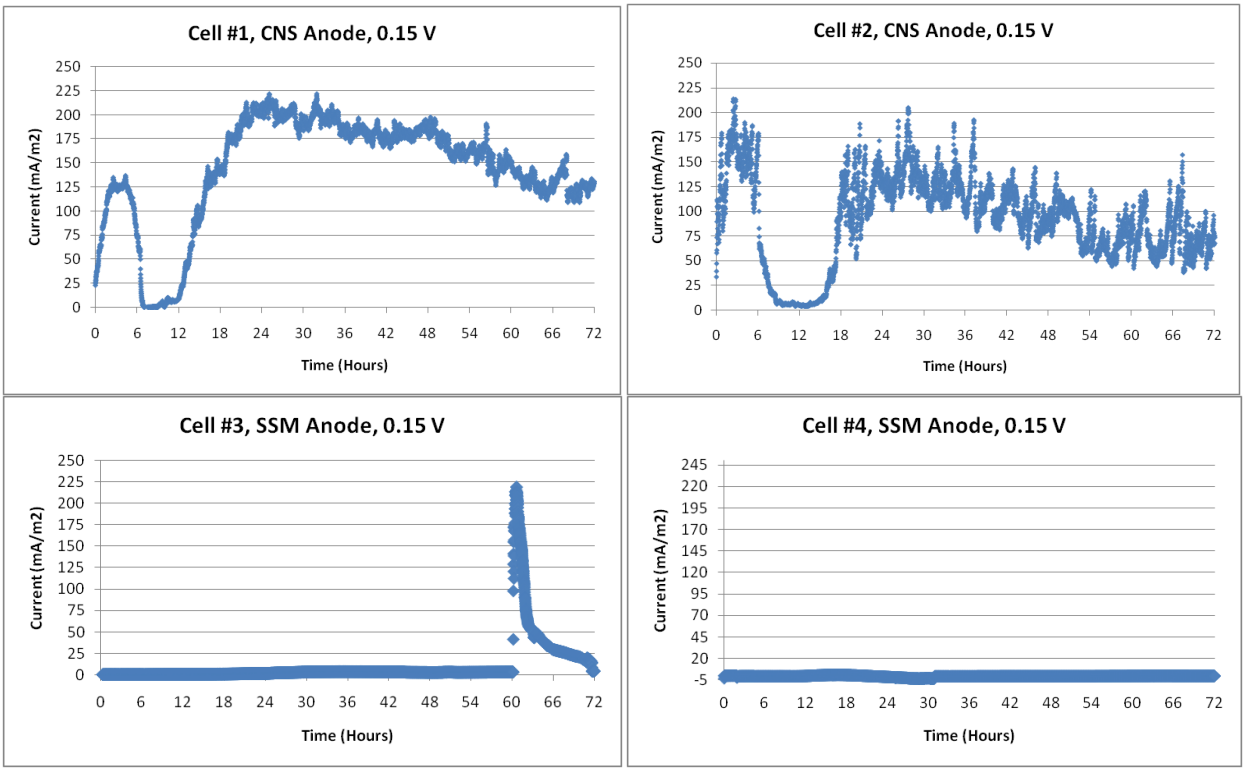

Figure 5.6. Potentiostatic data from all MiFCs tested during Trial 1 of the Pseudo-Sterile Experiment.

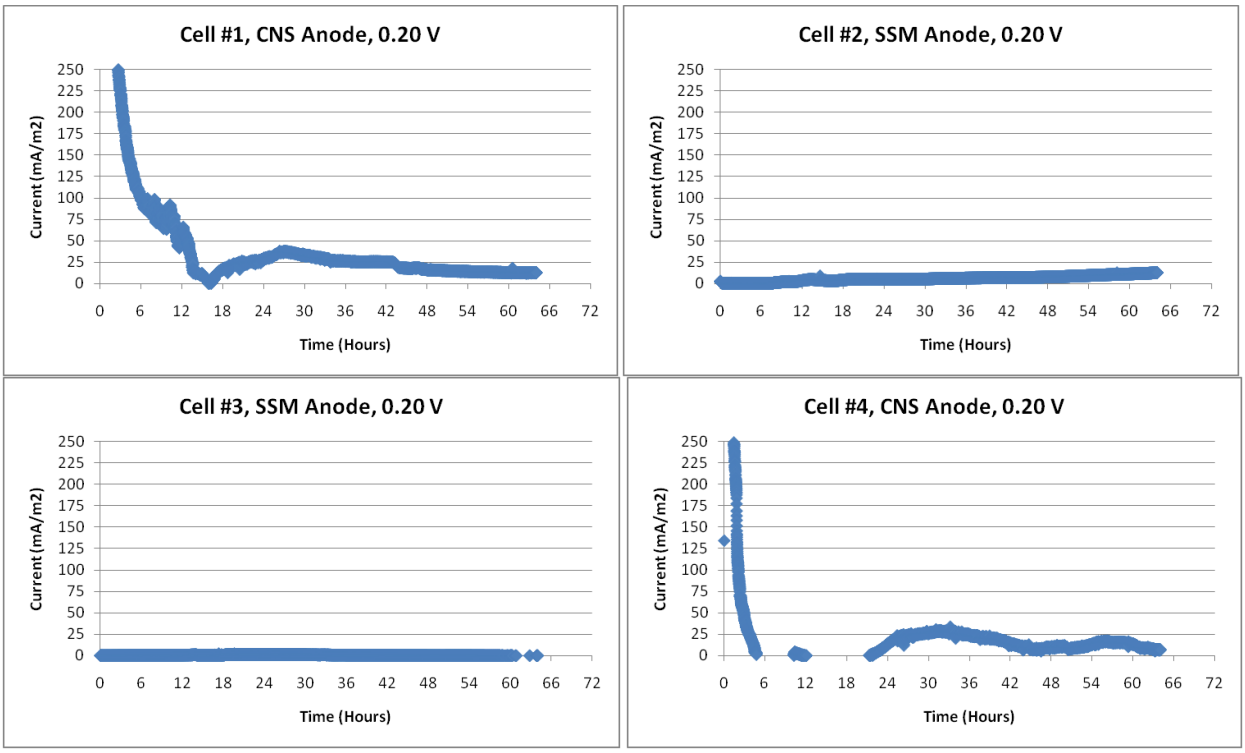

Figure 5.7. Potentiostatic data from all MiFCs tested during Trial 2 of the Pseudo-Sterile Experiment.

The shape of the potentiostatic curves was a first indication that the experiment was not completely sterile, but pseudo-sterile. After Trial #2, a small sample from the bulk fluid chamber of each fuel cell was observed under a florescent microscope to look for the presence of microorganisms. **Figure 5.8** below shows images from samples from each MiFC in Trial #2. In each image, microbial cells are visible, confirming the theory that microorganisms were present during the experiment. This information also helps to explain the trend in the potentiostatic data discussed previously.

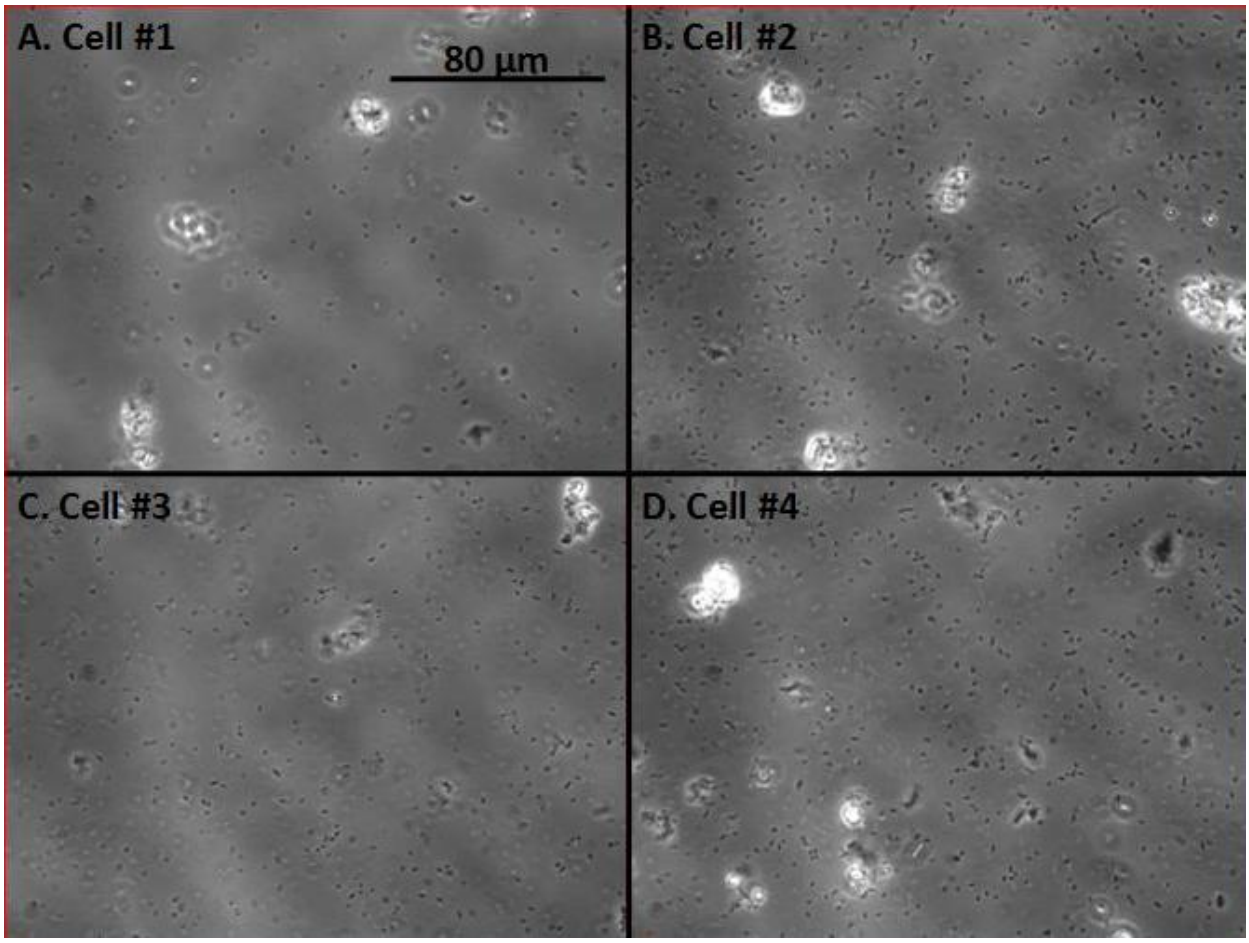

Figure 5.8. Florescent microscope images of samples of the MiFCs in Trial 2 of the Pseudo-Sterile Experiment. (A) and (D) represent samples taken from MiFCs with CNS-coated anodes, while (B) and (C) represent samples taken from MiFCs with uncoated anodes.

The Pseudo-Sterile Experiment was meant to quantify the current production from MiFCs containing sterile media in order to show that the power production from inoculated MiFCs was due solely to microbial activity. Although there was a detectable amount of biological contamination and consequently a small amount of power production during the experiment, the density of biomass (and the power production) was small in comparison to that of inoculated MiFCs. *It can therefore be concluded that the media by itself does not contribute a significant amount of power during the batch operation of the MiFCs in this study.*

5.3 LABORATORY SLUDGE MIFC TESTING RESULTS

A summary of the results of the first anaerobic experiment conducted using laboratory sludge discussed in **Section 3.1.1** can be found in **Table 5.3** below.

Table 5.3. Summary of Laboratory Sludge Testing Results.

Trial	Anode Type[a,b]	Cell No.	Voltage (V)	Maximum Current (mA m^{-2})	Maximum Power (mW m^{-2})
1	SSM	1	0.25	28.1	7.03
		2	0.25	12.1	3.02
	CNS	3	0.25	1150	288
		4	0.25	71.5	17.9
2	SSM	1	0.25	22.5	5.62
		3	0.25	303	75.6
	CNS	2	0.25	1820	455
		4	0.25	2020	506

[a] **SSM = uncoated stainless steel mesh anode;** [b] **CNS = carbon nanostructure-coated stainless steel mesh anode**

The maximum power density achieved with 1000 mg-glucose L^{-1} media and laboratory sludge was 506 mW m^{-2} obtained from a MiFC containing a CNS-coated anode in Trial 2. The maximum power densities of CNS-coated anode fuel cells were up to two orders of magnitude larger than those of MiFCs with uncoated anodes (for three of the four MiFCs) and one to two orders of magnitude larger than the maximum power densities from the pseudo-sterile experiment. The polarization curves and potentiostatic data for each trial are given in the following figures. In one of the trials (Trial 1, Cell #4), the power production remained low for reasons that remain unclear.

The polarization curves taken immediately prior to the beginning of the potentiostatic tests from Trial 1 and Trial 2 are given in **Figures 5.9** and **5.10** respectively. As was observed in the Pseudo-Sterile Experiment, the MiFCs with CNS-enhanced anodes outperformed the MiFCs with uncoated anodes even before the microorganisms had an opportunity to multiply significantly or form a biofilm on the anode.

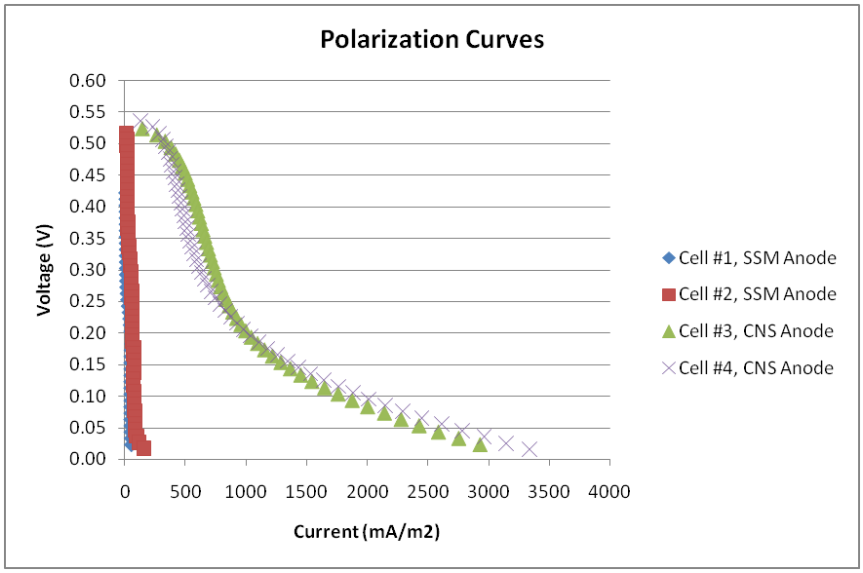

Figure 5.9. Polarization curves of all MiFCs tested during Trial 1 of the Laboratory Sludge Experiment.

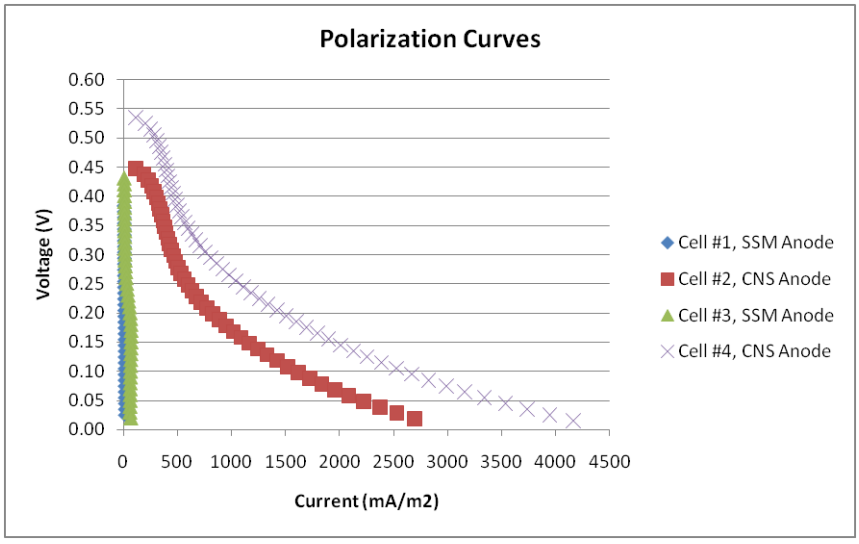

Figure 5.10. Polarization curves from all MiFCs tested during Trial 2 of the Laboratory Sludge Experiment.

The potentiostatic data from Trial 1 and Trial 2 are given in **Figures 5.11** and **5.12**. Arrows indicate the addition of glucose.

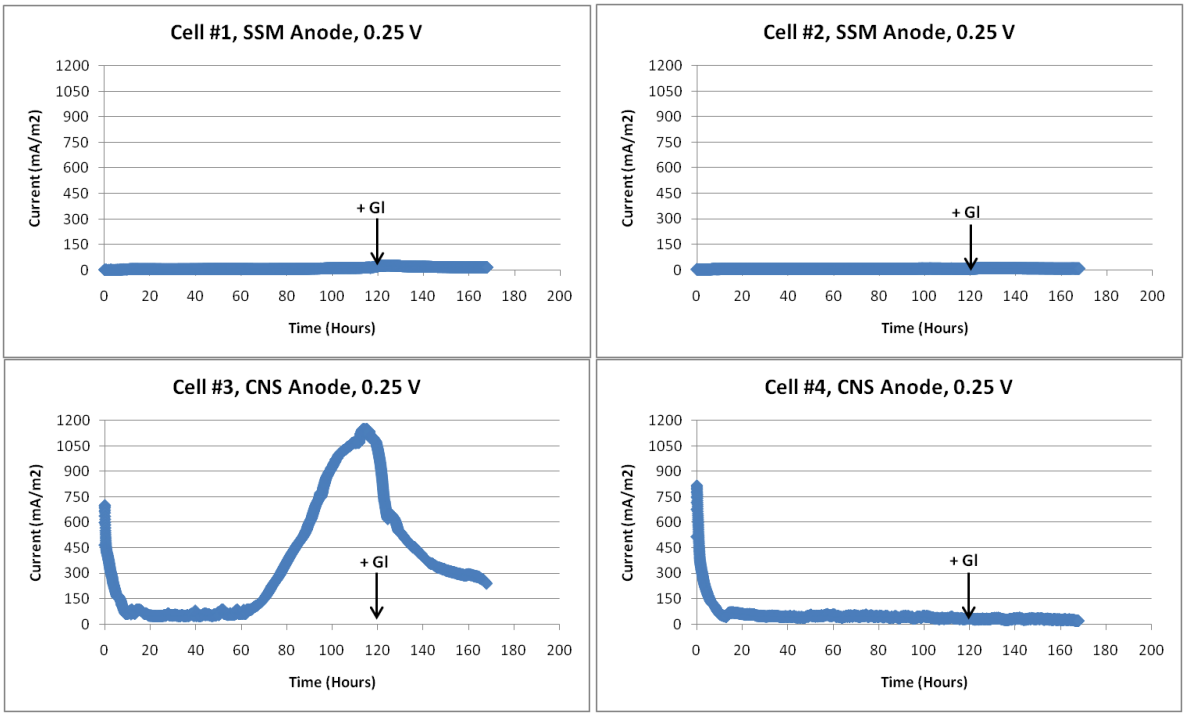

Figure 5.11. Potentiostatic data from all MiFCs tested during Trial 1 of the Laboratory Sludge Experiment.

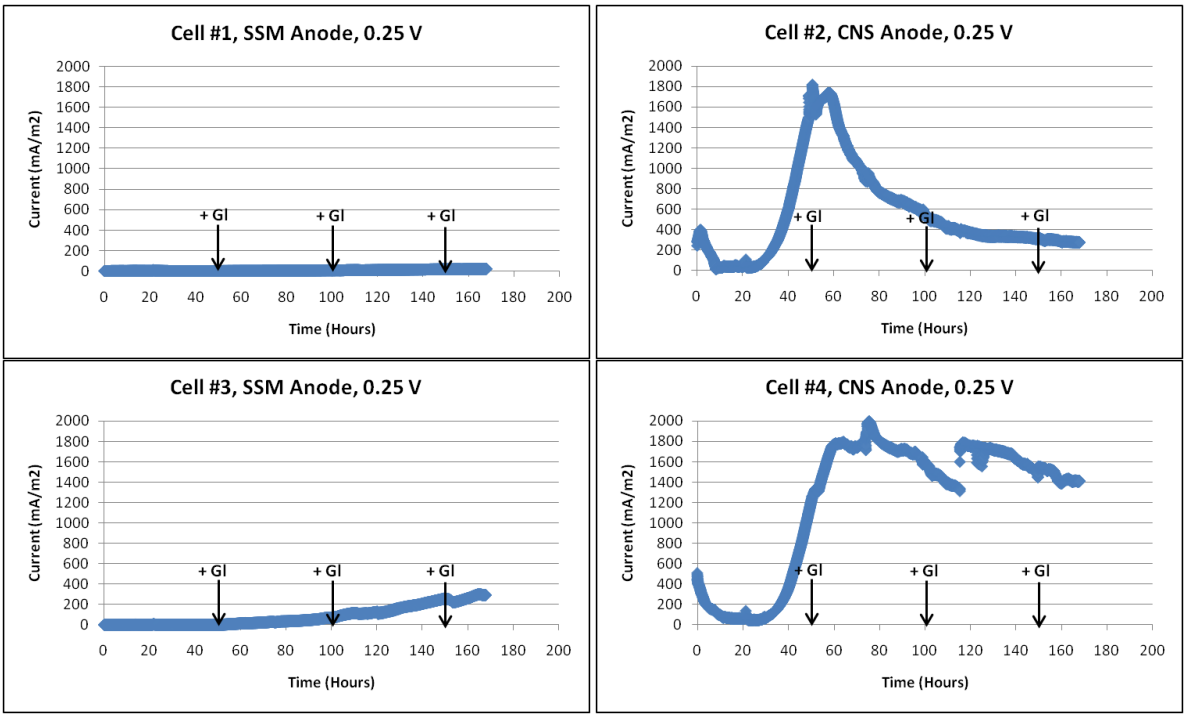

Figure 5.12. Potentiostatic data from all MiFCs tested during Trial 2 of the Laboratory Sludge Experiment.

All of the fuel cells were tested for one week at a voltage of 0.25 V (approximately one-half of the average open circuit voltage). Three of the four MiFCs with CNS-coated anodes tested in the two trials (Cell #3 in Trial 1 and Cells #2 and #4 in Trial 2) exhibited the same trend in current production observed during the Pseudo-Sterile Experiment. After an initial spike, the current density rose slowly to a maximum as the microorganisms grew and began to deposit electrons on the anode, and then decreased as the experiment progressed. The current density began to rise around hour 60 (day three) of the experiment in Trial 1, and hour 30 (the beginning of day two) in Trial 2. The sharp rise indicates that once the microorganisms acclimate to environment of the MiFC, the current density increases drastically. One hypothesis is that the formation of a biofilm directly on the MiFC anode is responsible for these results – the surface alteration of the CNS-coated anodes somehow promotes the growth of a biofilm while either the biofilm forms at a slower rate or does not form at all on uncoated anodes.

As a means to investigate this hypothesis, sections of each of the anodes from the MiFCs in Trial 2 were studied under an environmental scanning electron microscope (ESEM) (**Figure 5.14**). These sections were compared with each other and with images of CNS-coated and uncoated anodes before placement in a MiFC (**Figure 5.13**). It is interesting to note the increased amount of biomass attachment on the CNS-coated anodes in comparison with the uncoated anodes. These images help to support the hypothesis that biofilm formation is responsible for the differences in current and power production between MiFCs using CNS-coated and uncoated anodes. The images also support the theory that the surface alteration of flame-deposited carbon nanostructures on stainless steel mesh enhances its ability to attract and sustain microorganisms in a biofilm.

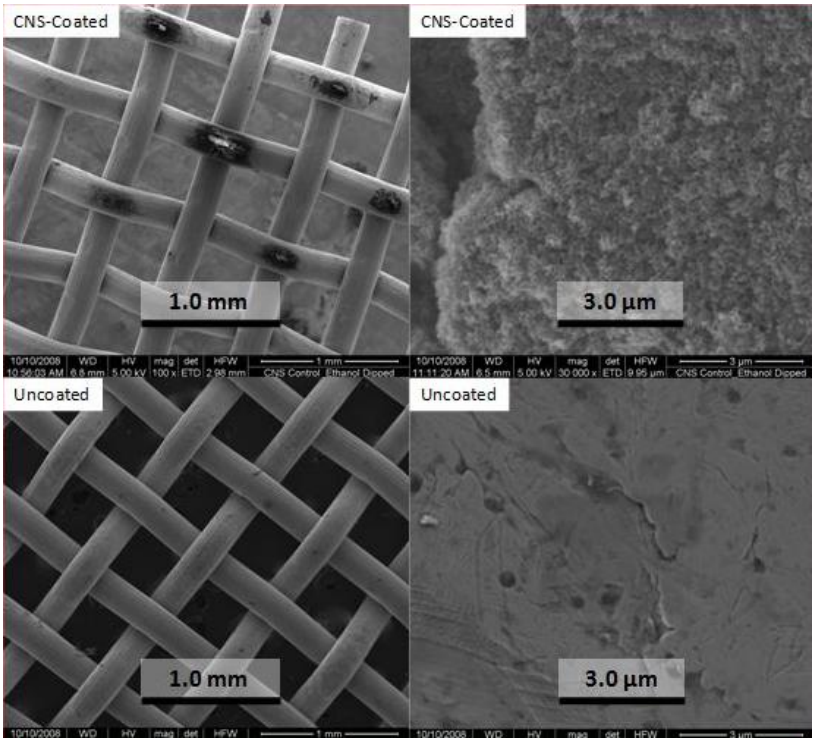

Figure 5.13. Scanning electron microscope (SEM) images of CNS-coated and uncoated stainless steel mesh anodes before placement in an MiFC at different magnifications.

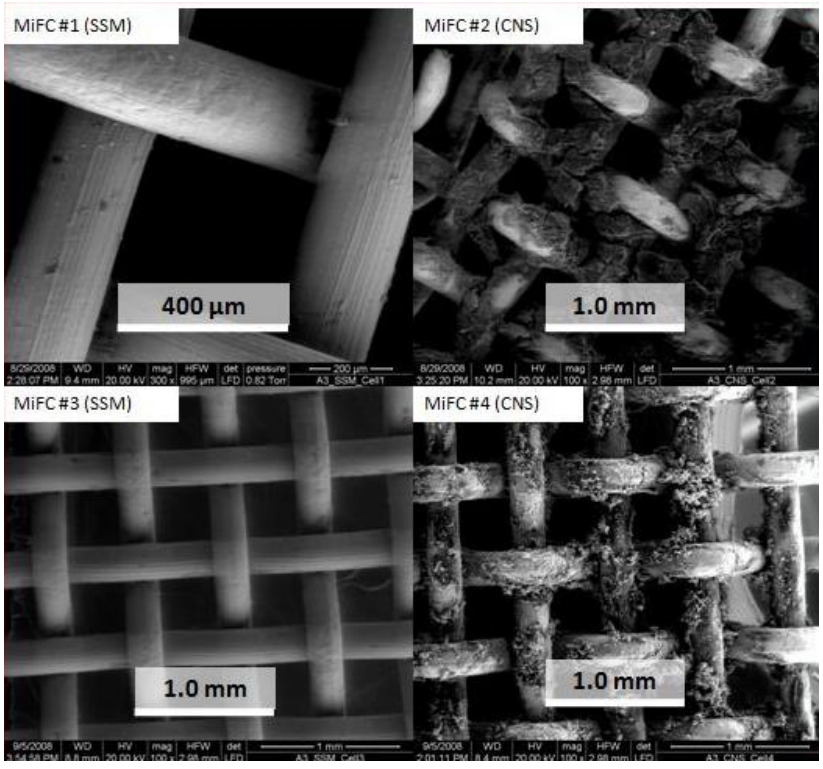

Figure 5.14. Scanning electron microscope (SEM) images of CNS-coated and uncoated anodes after the Trial 2 of the anaerobic sludge experiment. Note the increased biomass attachment on the CNS-coated anodes.

The Laboratory Sludge Experiment was the first experiment in this study to produce power from MiFCs inoculated with microorganisms. *The results provided significant evidence that coating a stainless steel mesh anode with carbon nanostructures improves the power density of MiFCs.* This conclusion can be drawn from the fact that MiFCs with altered anodes produced maximum power densities up to two orders of magnitude greater than unaltered anodes and that they were able to sustain power generation throughout the week-long test. The altered anodes were also able to attract biomass to form a biofilm to a greater extent than the plain anodes. Supplementary experimental results (particularly the Low-Iron, 3% Sludge Experiment discussed in **Section 5.6**) reinforce this conclusion.

5.4 SODIUM AZIDE MIFC TESTING RESULTS

The Sodium Azide Experiment was conducted using iron-rich sludge in order to show that without the presence of live microorganisms, the MiFCs would not be able to generate electrical current or power. Four MiFCs (all with CNS-coated anodes) were tested at 0.25 V for one week. Using the characteristic shape of the potentiostatic data produced by fuel cells with CNS-coated anodes from prior experiments (**Sections 5.2** and **5.3**) as a guide, the four cells were allowed to run normally until the first current density spike had subsided and the curve resembled the beginning of the steep current increase. This indicated that the microorganisms were active and had begun depositing electrons onto the anode. At this stage, 10 mM of sodium azide (NaN_3, a biological toxin) was added to each of two cells (volume approximately 140 mL) in order to see the effects of killing the microorganisms on the current density production.

The polarization curves taken prior to the beginning of the potentiostatic experiment are given below in **Figure 5.15**. As expected, each curve is similar in shape and magnitude as each

MiFC used the same anode material and size (6.5 cm^2 CNS-coated stainless steel mesh). The curves also resemble those from MiFCs with CNS-coated anodes in the Pseudo-Sterile and Laboratory Sludge Experiments (**Figures 5.4**, **5.5**, **5.9**, and **5.10**).

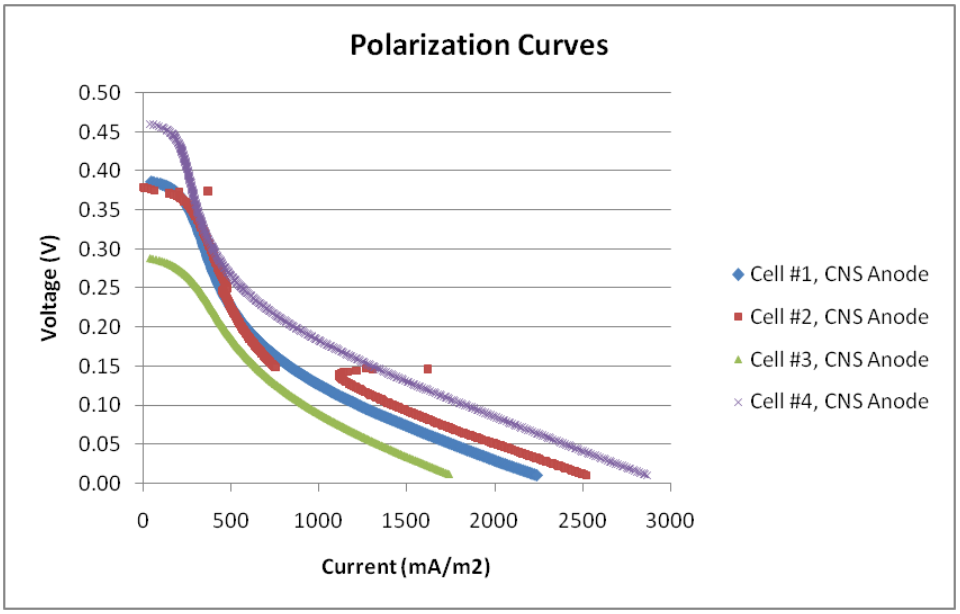

Figure 5.15. Polarization curves from all MiFCS tested during the Sodium Azide Experiment.

The potentiostatic results from this experiment are given in **Figures 5.16** and **5.17** below. Arrows indicate the addition of glucose. The first figure shows the potentiostatic curves from the week long test for all four fuel cells, while the latter shows a magnified version of the potentiostatic curves from the two fuel cells (Cells #1 and #2) supplemented with sodium azide.

As can be seen from the figures, the current density of all four MiFCs began rising between 80 and 100 hours (during day 4 and day 5) after the beginning of the experiment. Almost instantaneously upon supplementing Cells #1 and #2 with sodium azide, the current production fell steeply back to a low baseline value. These results provide supplementary

evidence that that the current production of the MiFCs in this study is due solely to the presence and effect of the active microorganisms.

The effect of fed-batch testing can also be seen in the potentiostatic curves of the two MiFCs not supplemented with sodium azide. In the potentiostatic curves of Cells #3 and #4 in **Figure 5.16**, one can observe a steady increase in current density from around hour 80 to a maximum peak which then declines and begins increasing again. This effect is due to the utilization of the electron donor (glucose) which causes the current density to fall once it is wholly consumed. The manual addition of more glucose at hour 142 results in a second region of increasing current density. If the experiment had been allowed to run longer, it would be expected that many of these cycles of increasing and decreasing current density would be visible as glucose was added to the MiFCs and utilized by the microorganisms.

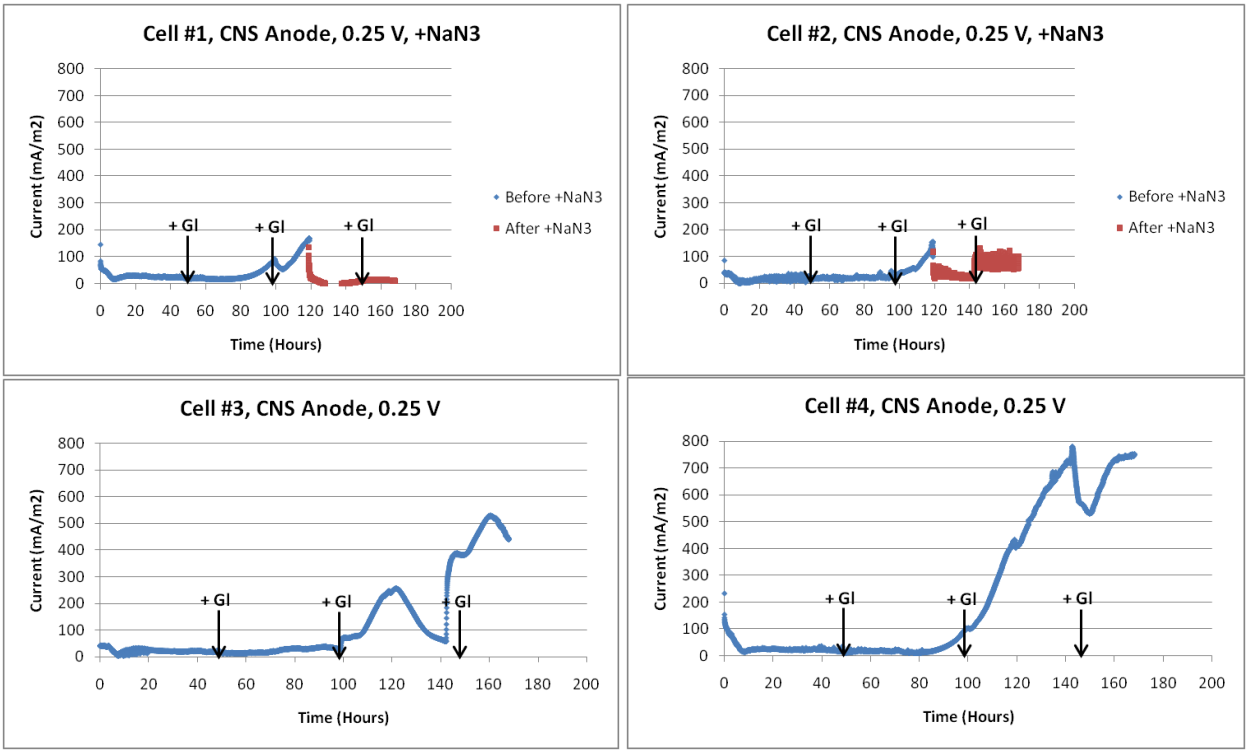

Figure 5.16. Potentiostatic data from all MiFCs tested during the Sodium Azide Experiment. MiFCs #1 and #2 were supplemented with 10mM of sodium azide while MiFCs #3 and #4 were allowed to continue uninhibited.

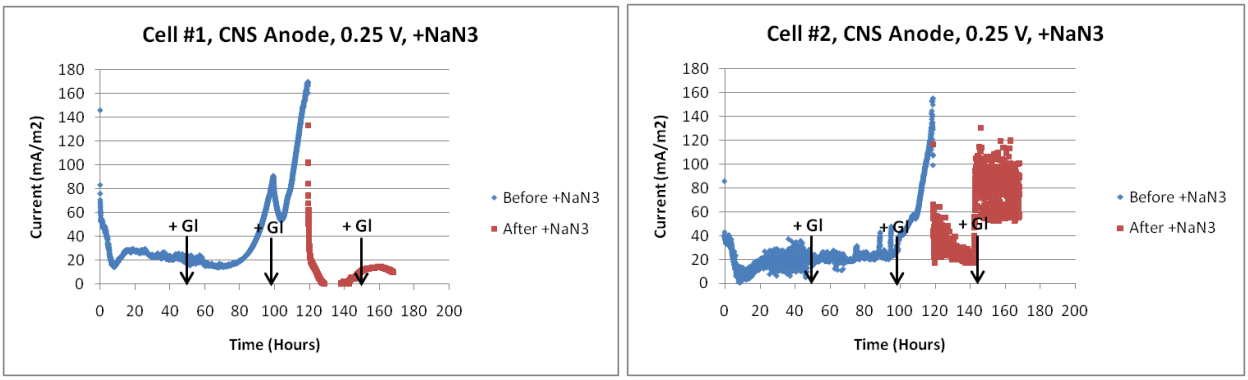

Figure 5.17. Potentiostatic data from MiFCs supplemented with 10 mM sodium azide during the Sodium Azide Experiment.

The Sodium Azide Experiment provided evidence that the current production in MiFCs used in this study could be attributed solely to active microorganisms. This information is critical in supporting the main hypothesis of this thesis; that CNS-coated anodes have the ability to promote higher power production in MiFCs by promoting biological growth and attachment. Without the knowledge that the current and power production of these fuel cells is due to microbial activity, there would not be a significant basis for assuming that some other electrochemical effect was not responsible for the increased current production of MiFCs containing CNS-coated anodes over those containing uncoated anodes.

5.5 IRON-RICH VS. CONTROL MEDIA MIFC TESTING RESULTS

The sludges used in the Laboratory Sludge Experiment as well as the Sodium Azide Experiment (iron-rich sludge) were both enriched with iron-rich media (see **Sections 3.1.1** and **3.1.2**). In order to determine whether placing the sludge in an iron-rich medium prior to inoculation of the MiFCs was necessary for current production, an experiment was conducted to compare the current density from MiFCs using sludge which had been placed in an iron-rich medium (**Table 3.1**), and sludge which had been placed in a control medium (**Table 3.2**, the

same medium used in the MiFC experiments). Six MiFCs were tested with CNS-coated anodes: three containing low-iron, 3% sludge and three containing iron-rich, 3% sludge.

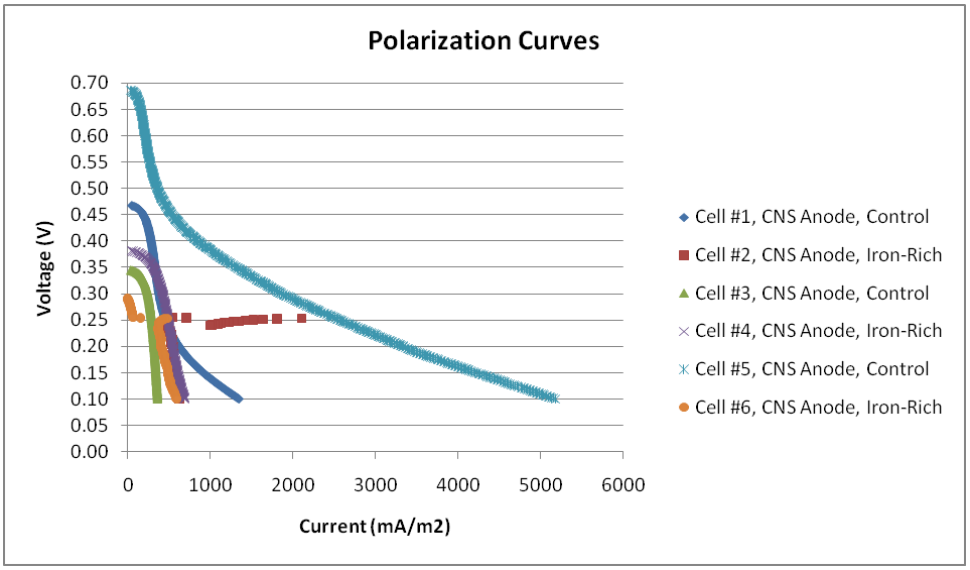

Figure 5.18. Polarization curves from all MiFCS tested during the Iron-Rich vs. Control Media Experiment.

The polarization curves from each MiFC recorded before the potentiostatic test are given above in **Figure 5.18** and the potentiostatic data is given below in **Figure 5.19**. Arrows indicate the addition of glucose.

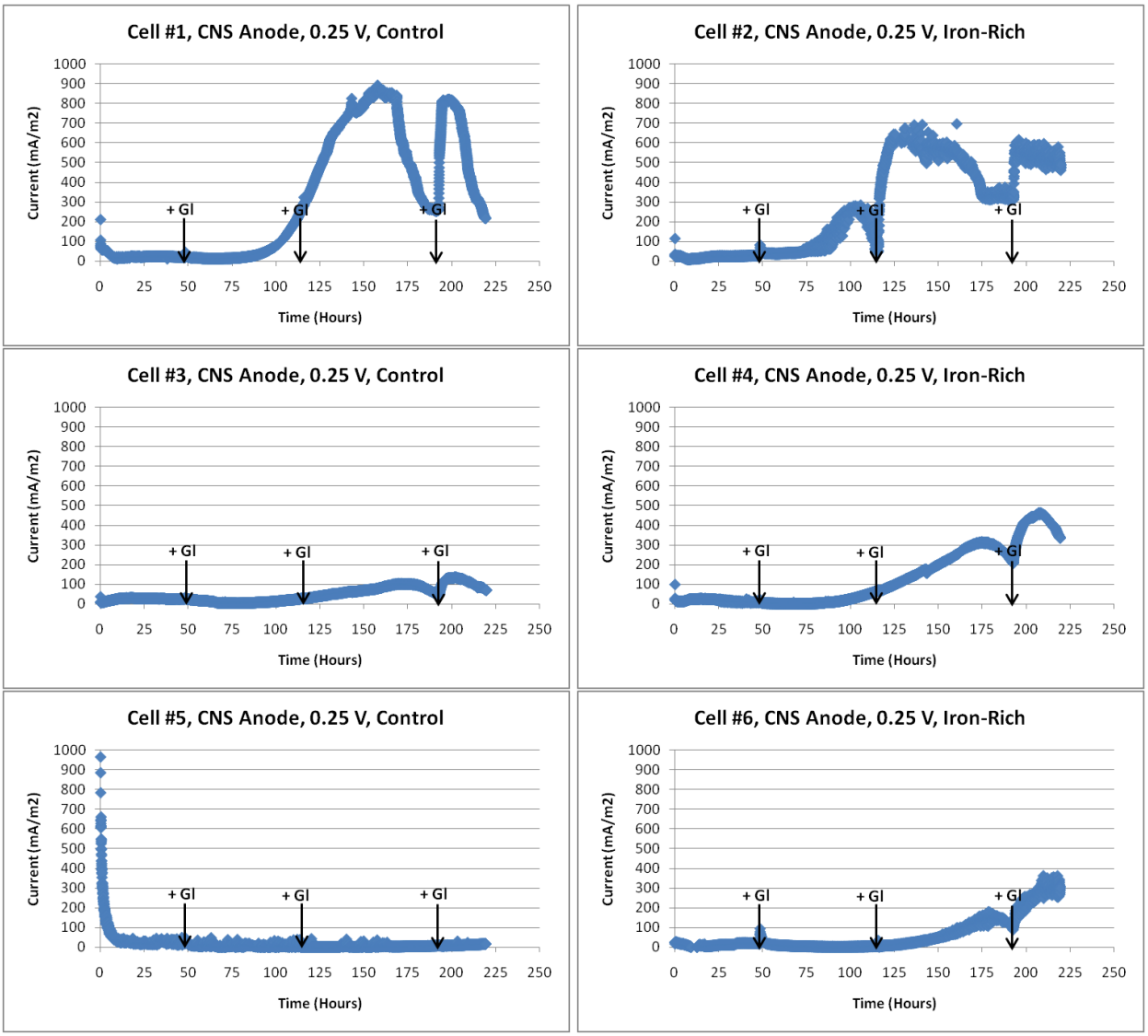

Figure 5.19. Potentiostatic data from all MiFCS tested during the Iron-Rich vs. Control Media Experiment.

From the potentiostatic data, one can see that Cell #1, which contained sludge that had been acclimated in control media, performed the best during the one-week test period. The next three best current producing MiFCs were the cells containing sludge in an iron-rich media (Cells #2, 4 and 6 in order). Cell #3 was lowest current producing MiFC of the experiment; Cell #5 never took off and will therefore not be considered in the comparison.

The same distinctive cycles visible in the potentiostatic curves from previous experiments are visible in this data. Glucose was added to the fuel cells every other day and corresponds to the recovery of current density production after it fell with the utilization of glucose.

The results of this experiment are not sufficient to conclude that keeping sludge in an iron-rich medium before the inoculation of MiFCs improved the resulting current density production of the fuel cells. In the absence of conclusive evidence that iron-enriched sludge performs better in MiFCs, the remaining experiments were conducted using low-iron, 3% sludge (the control sludge tested during this experiment).

5.6 LOW-IRON, 3% SLUDGE MIFC TESTING RESULTS

The Low-Iron, 3% Sludge Experiment was conducted using sludge that was not supplemented with additional iron (**Section 3.1.4**). A demonstration of the ability of MiFCs to run using unaltered samples from a wastewater treatment plant would be helpful in promoting MiFCs as a viable energy technology, as the fewer alterations (i.e. introduction of mediators, iron-enrichment, etc.) required to make the existing microorganisms produce power, the less the additional costs and complexity associated with the technology.

A brief summary of the maximum current and power densities of the six fuel cells in this experiment is given below in **Table 5.4**. As was seen in the Laboratory Sludge Experiment, the MiFCs with CNS-coated anodes generated power densities over two orders of magnitude greater than MiFCs using uncoated anodes and at least five times greater than the power density of the best performing MiFC in the Pseudo-Sterile Experiment (**Section 5.2**).

Table 5.4. Summary of Low-Iron, 3% Sludge Testing Results.

Anode Type[a,b]	Cell No.	Voltage (V)	Maximum Current (mA m^{-2})	Maximum Power (mW m^{-2})
CNS	1	0.25	720	180
	3	0.25	842	210
	5	0.25	641	160
SSM	2	0.25	11.4	2.85
	4	0.25	2.63	0.658
	6	0.25	3.92	0.980

[a] **SSM = uncoated stainless steel mesh anode;** [b] **CNS = carbon nanostructure-coated stainless steel mesh anode**

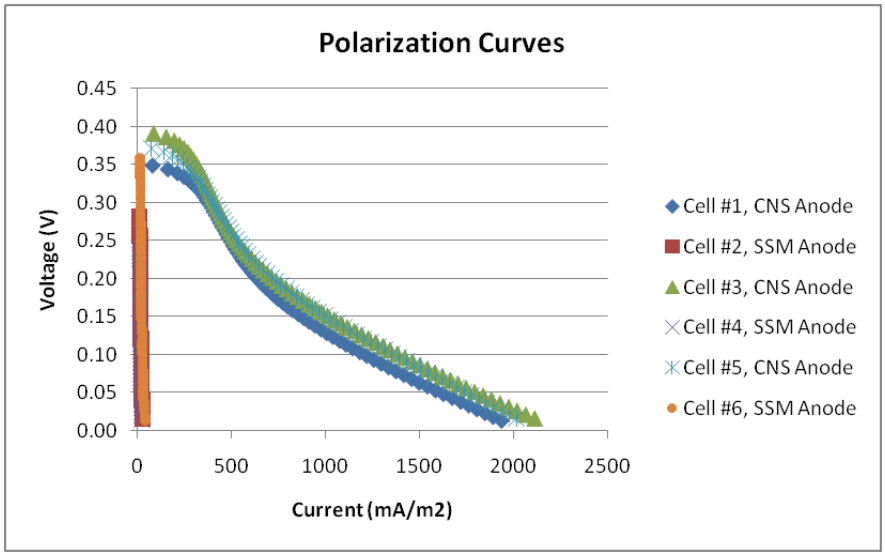

Figure 5.20. Polarization curves from all MiFCS tested during the Low-Iron, 3% Sludge Experiment.

The polarization curves from all six MiFCs taken prior to the beginning of the potentiostatic experiment (i.e. immediately after the fuel cells were inoculated) are given above in **Figure 5.20**. As was the result in the Pseudo-Sterile and Laboratory Sludge Experiments, the MiFCs containing CNS-coated anodes performed orders of magnitude better than MiFCs with

uncoated anodes, even before adequate time had passed for the microbial colony to grow and form a biofilm.

The results of the potentiostatic experiment (run for approximately eight days at 0.25 V) are shown in **Figure 5.21** below. Arrows indicate the addition of glucose.

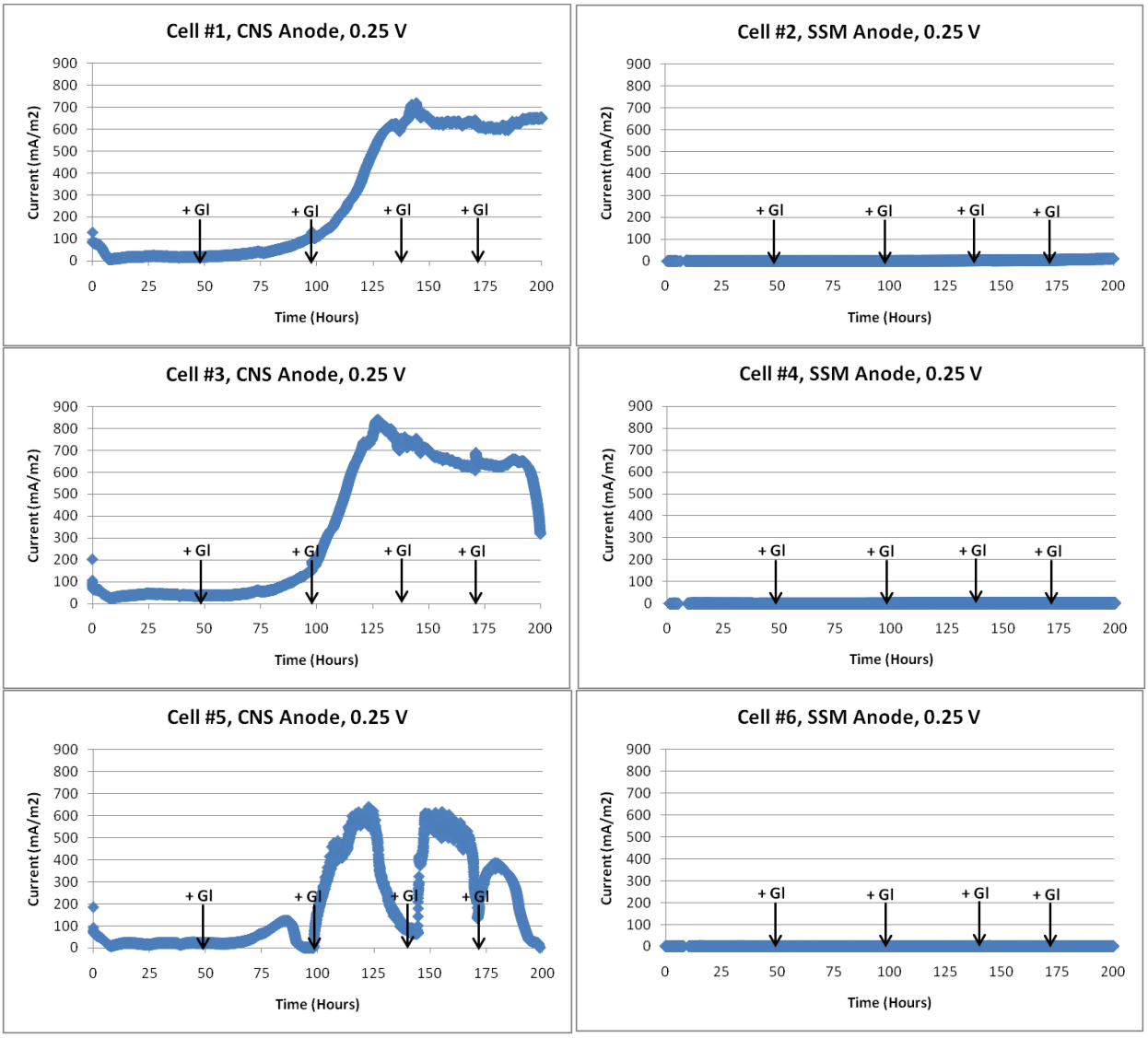

Figure 5.21. Potentiostatic data from all MiFCS tested during the Low-Iron, 3% Sludge Experiment.

A significant difference in the current density production between MiFCs with CNS-coated and uncoated anodes can be seen in the potentiostatic curves. The data also contains the same characteristic curves observed in previous experiments. The MiFCs with CNS-coated anodes began producing current at an increasing rate around hour 65 of experimentation, and reached a maximum value approximately 60 hours later.

Cell #5 is a clear example of the effect of fed-batch operation on the current density production. The shape of the curve implies that this MiFC may have utilized glucose at a faster rate than the other MiFCs. When glucose was added to the fuel cell (occurring every other day), the current density recovered rapidly.

The results of this experiment further support the hypothesis that flame-deposited carbon nanostructures can improve the current and power density production of MiFCs. The results also show that the MiFCs in this study can be powered with digester sludge from a wastewater treatment plant after acclimating to the MiFC without the need of additional chemical compounds.

5.7 NUMERICAL MODELING RESULTS

The numerical model described in **Chapter 4.0**, was implemented in Mathematica® (Wolfram Research, Inc.). The model was validated by replicating the results from Marcus et al. as depicted in **Appendix B**. The model was then run using anaerobic sludge data from the literature and experimental data from this study in order to compare model predictions to results obtained from the Laboratory Sludge Experiment (see **Section 5.3**) for a seven day simulation time. Values for microbial growth and kinetic parameters were taken from the literature and the maximum specific rate of ED utilization (q_{max}) was adjusted to match the peak current density

and the shape of the current density curve in the model results to the experimental data. **Table 5.5** summarizes the modeling parameters which best matched the experimental data.

Table 5.5. Modeling Parameters.

Parameter	Symbol	Value	Units	Reference
Electron equivalence of glucose	γ_1	24.0	mmol e^- mmol-gl^{-1}	[61]
Electron equivalence of active biomass	γ_2	0.177	mmol e^- mg-VSS^{-1}	[62]
Glucose diffusion coefficient	$D_{ED,l}$	0.579	cm^2 day^{-1}	[63]
Glucose diffusion coefficient in biofilm	$D_{ED,f}$	0.463	cm^2 day^{-1}	[62]
Half-max-rate glucose concentration	K_{sd}	2.621×10^{-5}	mmol cm^{-3}	[64]
Maximum specific rate of ED utilization	q_{max}	0.074, 0.090*	mmol-gl mg-VSS^{-1} day^{-1}	--
True yield	Y	13.437	mg-VSS mmol-gl^{-1}	[64]
Inactivation decay coefficient for active biomass	b_{ina}	0.05	day^{-1}	[62]
Endogenous decay coefficient for active biomass	b_{res}	0.05	day^{-1}	[62]
Rate of biomass loss due to detachment	b_{det}	0.10	day^{-1}	[4]
Fraction of electrons from glucose used for energy generation	fe^0	0.90	--	[4]
Conductivity of biofilm matrix	k_{bio}	0.0001	mS cm^{-1}	[4]
Density of active biomass	$X_{f,a}$	200	mg-VSS cm^{-3}	[4]
Density of inactive biomass	$X_{f,i}$	200	mg-VSS cm^{-3}	[4]
Anode potential	V_{anode}	0.50	V	measured

***Adjusted from initial value of 0.238 [64] from literature to match experimental data.**

The model was run with two different values of q_{max}: one which best matched the first section of the experimental data (0.090 mmol mg-VSS^{-1} day^{-1}) and one which best matched the steady portion (0.074 mmol mg-VSS^{-1} day^{-1}). **Figures 5.22** and **5.27** show the best fit of the model using the parameters listed above to the results of Laboratory Sludge Experiment, Trial 2, Cell #4. Glucose concentrations measured during the experiment were used as the bulk concentration of electron donor in the model. **Figures 5.23** and **5.28**, **5.24** and **5.29,** and **5.25**

and **5.30** are the biomass fractions, local potential and current, and electron donor (glucose) concentrations in the biofilm at the end of the one-week simulation respectively. **Figures 5.26** and **5.31** show the bulk glucose concentration (measured during the experiment) versus the current production from the model over time.

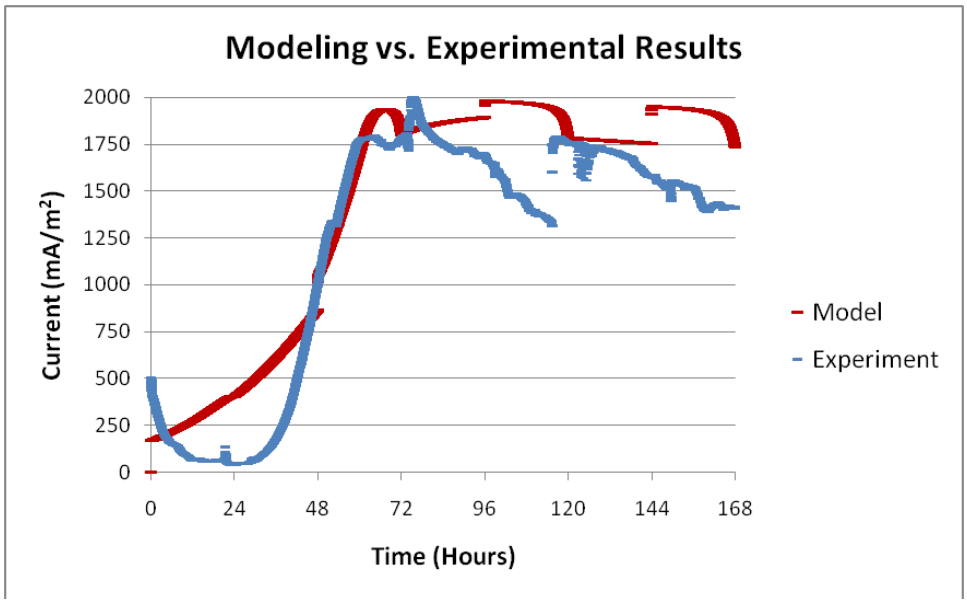

Figure 5.22. Best-fit modeling results to Cell #4 from Trial 2 of the Laboratory Sludge Experiment with q_{max} = 0.090 mmol mg-VSS^{-1} day^{-1}.

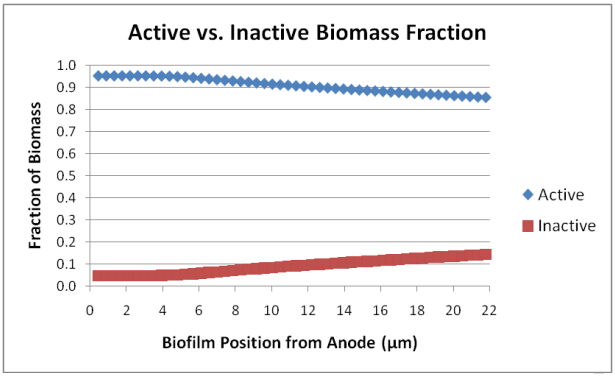

Figure 5.23. Biomass fraction in biofilm modeling results with q_{max} = 0.090 mmol mg-VSS^{-1} day^{-1}at the last time step.

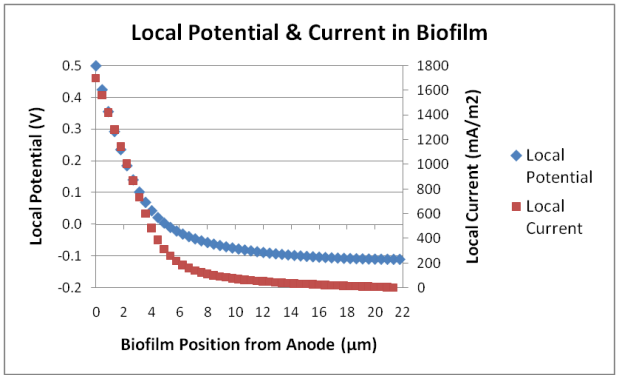

Figure 5.24. Local potential and current in biofilm modeling results with q_{max} = 0.090 mmol mg-VSS^{-1} day^{-1} at the last time step.

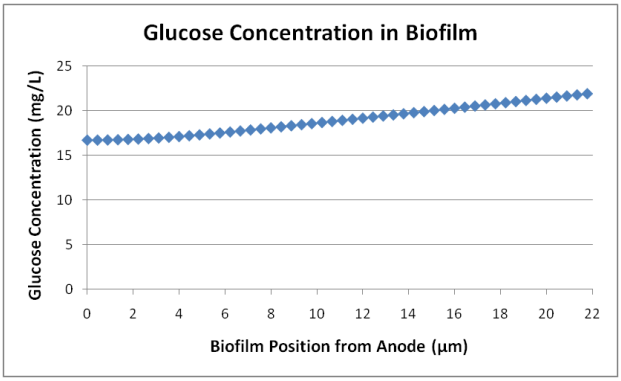

Figure 5.25. Biofilm glucose concentration modeling results with q_{max} = 0.090 mmol mg-VSS^{-1} day^{-1}at the last time step.

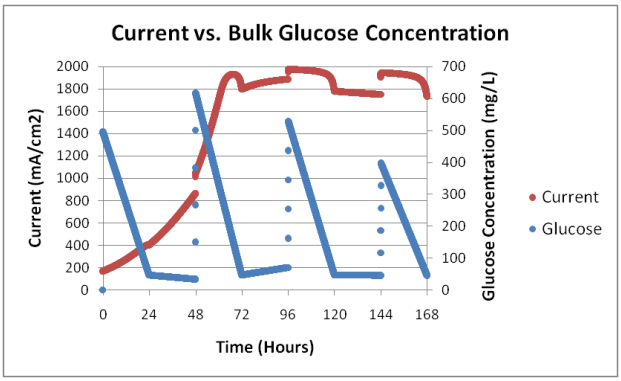

Figure 5.26. Current production vs. bulk glucose concentration modeling results with q_{max} = 0.090 mmol mg-VSS^{-1} day^{-1}.

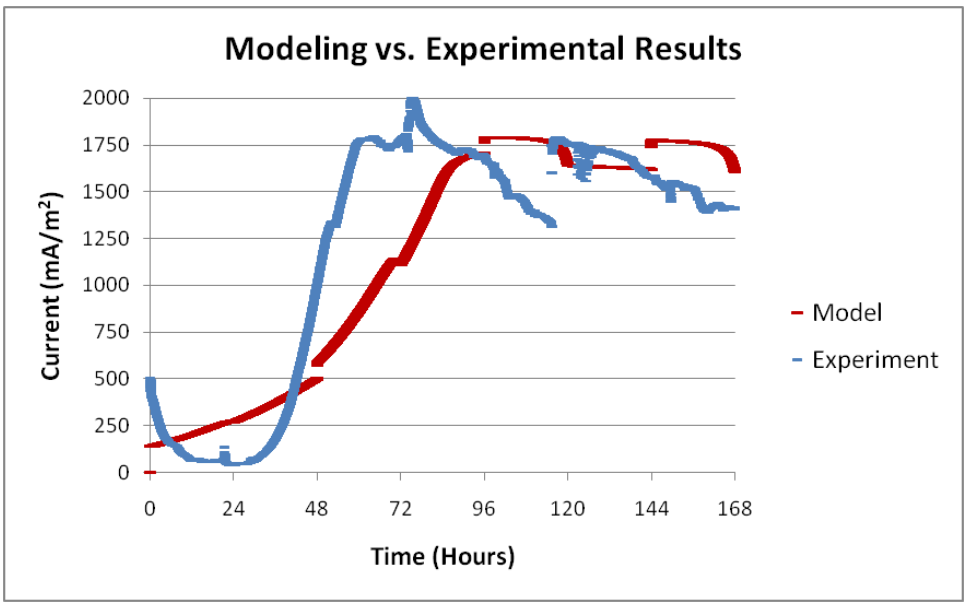

Figure 5.27. Best-fit modeling results to Cell #4 from Trial 2 of the Laboratory Sludge Experiment with q_{max} = 0.074 mmol mg-VSS^{-1} day^{-1}.

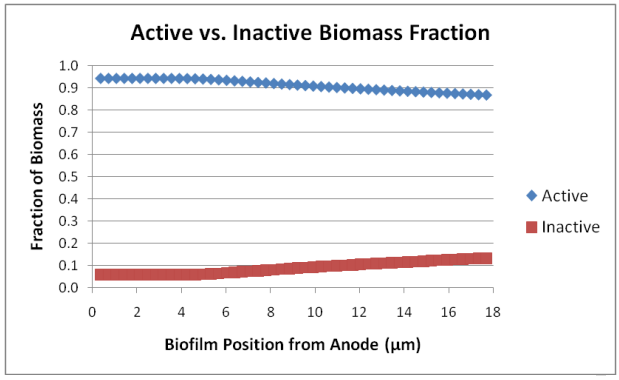

Figure 5.28. Biomass fraction in biofilm modeling results with q_{max} = 0.074 mmol mg-VSS^{-1} day^{-1} at the last time step.

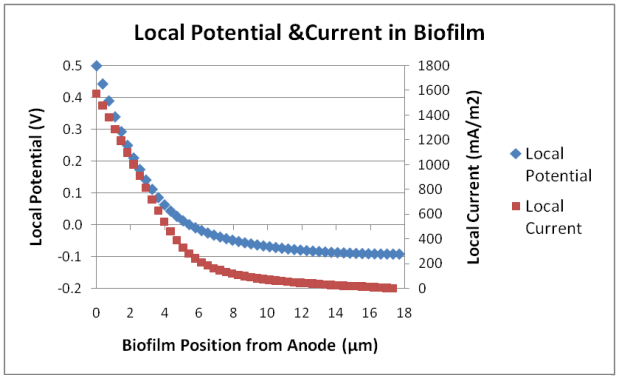

Figure 5.29. Local potential and current in biofilm modeling results with q_{max} = 0.074 mmol mg-VSS^{-1} day^{-1} at the last time step.

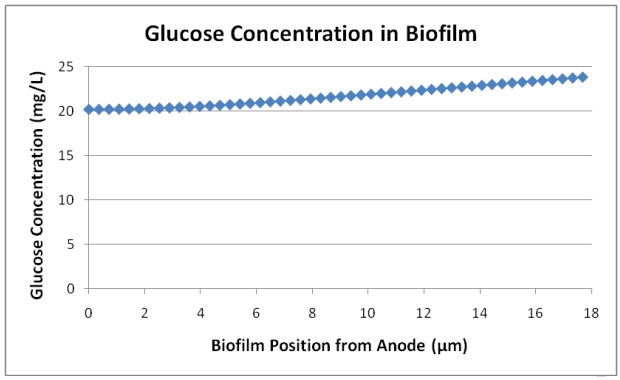

Figure 5.30. Biofilm glucose concentration modeling results with q_{max} = 0.074 mmol mg-VSS^{-1} day^{-1} at the last time step.

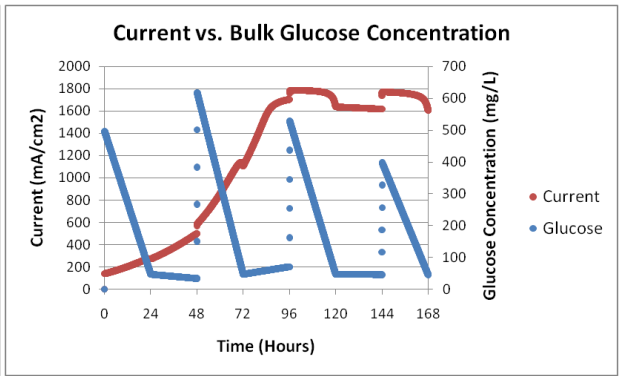

Figure 5.31. Current production vs. bulk glucose concentration modeling results with q_{max} = 0.074 mmol mg-VSS^{-1} day^{-1}.

A brief summary of the modeling results for the two cases presented in the prior figures is given below in **Table 5.6**.

Table 5.6. Summary of Modeling Results.

Source	q_{max} mmol-gl mg-VSS^{-1} day^{-1}	Biofilm Thickness (μm)	Maximum Current (mA m^{-2})
Numerical Model	0.090	21.8	1980
	0.074	17.7	1790
Laboratory Sludge Experiment	--	--	2020

The maximum specific rate of electron donor utilization (q_{max}) was adjusted from the original value taken from literature for anaerobic sludge to fit the experimental data. Although the values used in the model (0.074 and 0.090 mmol-gl mg-VSS^{-1} day^{-1}) are approximately one-third of the original value taken from the literature (0.238 mmol-gl mg-VSS^{-1} day^{-1}), they still lie within the range of observed values [65].

From **Figures 5.22 and 5.27**, the model run for a q_{max} value of 0.090 mmol mg-VSS^{-1} day^{-1} provides a reasonable prediction of both the magnitude of the maximum current generation (~2000 mA/m^2) and the time to onset of maximum current generation (~72 hours). With a q_{max} value of 0.074 mmol mg-VSS^{-1} day^{-1} the model provides a reasonable prediction of both the "steady" current generation (1300 – 1750 mA/m^2) and the time to onset of "steady" current generation (~96 hours). The model has difficulty in predicting both portions of the experiment using a single set of parameters. This may be caused by the fact that the Marcus model was originally based on a MiFC with a constant bulk electron donor concentration and that it may not

be able to effectively capture the current generation during start-up of a fed-batch system. The model cannot capture the dynamics of current production during the initial 36 hours when the cell exhibits an initially higher than predicted current, followed by a "U" shaped drop and recovery in current production. The phenomena leading to this behavior is not presently understood or captured in the model description. Finally, the model appears to be less sensitive to the glucose concentration than the actual cell. As shown in **Figs. 5.26** and **5.31**, the model predicts that the glucose concentration goes to a very low value with a relatively small effect on the current output. On the other hand, the experimental results show a significant drop and recovery with the glucose depletion/addition cycles. Overall, the Marcus model can predict the magnitude and time-to-onset of maximum current and steady current using accepted values for kinetic parameters and adjustment of only one parameter (the maximum specific rate of ED utilization). This represents an encouraging starting point for the development of a more comprehensive MIFC modeling effort.

6.0 CONCLUSIONS AND FUTURE WORK

A brief summary of the results of biotic MiFC tests comparing the use of CNS-coated and uncoated anodes is provided below in **Table 6.1**.

Table 6.1. Summary of Biotic MiFC Test Results Comparing the Effect of Anode Type.

Anode Type[a,b]	Experiment	Voltage (V)	Maximum Current (mA m^{-2})	Maximum Power (mW m^{-2})
CNS	Laboratory Sludge	0.25	1150	288
		0.25	71.5	17.9
		0.25	1820	455
		0.25	2020	506
	Low-Iron, 3% Sludge	0.25	720	180
		0.25	842	210
		0.25	641	160
SSM	Laboratory Sludge	0.25	28.1	7.03
		0.25	12.1	3.02
		0.25	22.5	5.62
		0.25	303	75.6
	Low-Iron, 3% Sludge	0.25	11.4	2.85
		0.25	2.63	0.658
		0.25	3.92	0.980

[a] SSM = uncoated stainless steel mesh anode; [b] CNS = carbon nanostructure-coated stainless steel mesh anode

With the exception of two fuel cells during the Laboratory Sludge Experiment (one using a CNS-coated anode and one using an uncoated anode), all of the MiFCs with CNS-coated

anodes performed one to two orders of magnitude better than MiFCs with uncoated, plain stainless steel mesh anodes. The largest power density achieved in this study was 506 mW m^{-2}, with the average maximum power density of the CNS-enhanced MiFCs in the Laboratory Sludge and Low-Iron, 3% Sludge Experiments being 300 mW m^{-2} when neglecting the fuel cell which never generated sufficient power (Cell #4, Trial 1, Laboratory Sludge Experiment). In comparison, the average maximum power density of the MiFCs with uncoated anodes in the same two experiments was only 13.7 mW m^{-2}, an almost 22-fold reduction.

While the results of the Laboratory Sludge and Low-Iron, 3% Sludge Experiments provide compelling evidence that the surface deposition of carbon nanostructures onto stainless steel mesh anodes improves the power output of MiFCs, the Sodium Azide Experiment was also important in that it showed that the recorded power was derived from the activity of microorganisms. This information is crucial in proving that the presence of carbon nanostructures on a MiFC anode improves the power generation of the fuel cells by affecting the growth and electron transfer of microorganisms, and not by an electrochemical effect caused by the presence of the nanostructures.

Several future studies into the use of CNS-coated anodes in MiFCs would be beneficial to form a more detailed conclusion of their effect on power production. First, a study to determine the actual (microscopic) surface area of CNS-coated anodes would allow for a better comparison of current and power density production to uncoated anodes. Most of the performance data on MiFCs is reported based on the projected surface area of the anode, and the possibility exists that the increased power production is due in part to an increase in surface area corresponding to the addition of carbon nanostructures. Second, a study of the effect of carbon nanostructures on altering the surface properties of stainless steel mesh would provide a better understanding of the

effect of anode surface properties on biofilm formation. As seen in **Figure 5.14**, CNS-coated anodes attracted a much larger amount of biomass to the anode surface. If the cause of this phenomenon was known, it could be applied to other types of MiFC anodes to increase power output. Third, further studies into the method of electron transfer in MiFC biofilms would go a long way in supporting the hypothesis that the formation of a biofilm on the CNS-anode is responsible for the ensuing power density improvement.

This study shows that flame deposited carbon nanostructures show promise as surface enhancements for microbial fuel cell anodes. The improved current and power densities achievable with these anodes could help to bring MiFCs into use as a new, renewable energy technology.

REFERENCES

1. Naha, S., *Growth Model, Synthesis of Carbon Nanostructures and Alteration of Surface Properties Using Them*, in *Department of Engineering Science and Mechanics*. 2008, Virginia Polytechnic Institute and State University: Blacksburg, VA. p. 135.

2. O'Hayre, R., et al., *Fuel Cell Fundamentals*. 2006, Hoboken, New Jersey: John Wiley & Sons, Inc. 409.

3. Rabaey, K., et al., *A microbial fuel cell capable of converting glucose to electricity at high rate and efficiency.* Biotechnology Letters, 2003. **25**(18): p. 1531-1535.

4. Marcus, A.K., C.I. Torres, and B.E. Rittmann, *Conduction-based modeling of the biofilm anode of a microbial fuel cell.* Biotechnology and Bioengineering, 2007. **98**(6): p. 1171-1182.

5. Logan, B.E., *Microbial Fuel Cells*. 2008, Hoboken, New Jersey: John Wiley & Sons, Inc. 200.

6. Potter, M.C., *Electrical Effects Accompanying the Decomposition of Organic Compounds.* Proceedings of the Royal Society of London. Series B, Containing Papers of a Biological Character, 1911. **84**(571): p. 260-276.

7. Davis, J.B. and H.F. Yarbrough, Jr., *Preliminary Experiments on a Microbial Fuel Cell.* Science, 1962. **137**(3530): p. 615-616.

8. Madigan, M.T. and J.M. Martinko, *Brock Biology of Microorganisms*. 11th ed. 2006, Upper Saddle River, NJ: Pearson Education, Inc.

9. Logan, B.E. and J.M. Regan, *Electricity-producing bacterial communities in microbial fuel cells.* Trends in Microbiology, 2006. **14**(12): p. 512-518.

10. Logan, B.E., et al., *Microbial Fuel Cells: Methodology and Technology.* Environ. Sci. Technol., 2006. **40**(17): p. 5181-5192.

11. Park, D.H. and J.G. Zeikus, *Utilization of Electrically Reduced Neutral Red by Actinobacillus succinogenes: Physiological Function of Neutral Red in Membrane-Driven Fumarate Reduction and Energy Conservation.* J. Bacteriol., 1999. **181**(8): p. 2403-2410.

12. Park, D.H. and J.G. Zeikus, *Electricity Generation in Microbial Fuel Cells Using Neutral Red as an Electronophore.* Appl. Environ. Microbiol., 2000. **66**(4): p. 1292-1297.

13. Bond, D.R., et al., *Electrode-Reducing Microorganisms That Harvest Energy from Marine Sediments.* Science, 2002. **295**(5554): p. 483-485.

14. Lovley, D.R., et al., *Humic substances as electron acceptors for microbial respiration.* Nature, 1996. **382**(6590): p. 445-448.

15. Newman, D.K. and R. Kolter, *A role for excreted quinones in extracellular electron transfer.* Nature, 2000. **405**(6782): p. 94-97.

16. Rabaey, K., et al., *Biofuel Cells Select for Microbial Consortia That Self-Mediate Electron Transfer.* Appl. Environ. Microbiol., 2004. **70**(9): p. 5373-5382.

17. Kim, H.J., et al., *A mediator-less microbial fuel cell using a metal reducing bacterium, Shewanella putrefaciens.* Enzyme and Microbial Technology, 2002. **30**: p. 145-152.

18. Kim, B.H., et al., *Direct Electrode Reaction of Fe(III)-Reducing Bacterium, Shewanella putrefaciens.* J. Microbiol. Biotechnol., 1999. **9**(2): p. 127-131.

19. Kim, H.J., et al., *A Microbial Fuel Cell Type Lactate Biosensor Using a Metal-Reducing Bacterium, Shewanella putrefaciens.* Journal of Microbiology and Biotechnology, 1999. **9**(3): p. 365-367.

20. Myers, C.R. and J.M. Myers, *Localization of cytochromes to the outer membrane of anaerobically grown Shewanella putrefaciens MR-1.* J. Bacteriol., 1992. **174**(11): p. 3429-3438.

21. Bond, D.R. and D.R. Lovley, *Electricity Production by Geobacter sulfurreducens Attached to Electrodes.* Appl. Environ. Microbiol., 2003. **69**(3): p. 1548-1555.

22. Gorby, Y.A., et al., *Electrically conductive bacterial nanowires produced by Shewanella oneidensis strain MR-1 and other microorganisms* Proceedings of the National Academy of Sciences of the United States of America, 2006. **103**(30): p. 11358-11363.

23. Reguera, G., et al., *Extracellular electron transfer via microbial nanowires.* Nature, 2005. **435**(7045): p. 1098-1101.

24. You, S., et al., *A microbial fuel cell using permanganate as the cathodic electron acceptor.* Journal of Power Sources, 2006. **162**(2): p. 1409-1415.

25. Venkata Mohan, S., et al., *Bioelectricity production from wastewater treatment in dual chambered microbial fuel cell (MFC) using selectively enriched mixed microflora: Effect of catholyte.* Bioresource Technology, 2008. **99**(3): p. 596-603.

26. Min, B., S. Cheng, and B.E. Logan, *Electricity generation using membrane and salt bridge microbial fuel cells.* Water Research, 2005. **39**(9): p. 1675-1686.

27. Erable, B., L. Etcheverry, and A. Bergel, *Increased power from a two-chamber microbial fuel cell with a low-pH air-cathode compartment.* Electrochemistry Communications, 2009. **11**(3): p. 619-622.

28. Logan, B.E., et al., *Electricity generation from cysteine in a microbial fuel cell.* Water Research, 2005. **39**(5): p. 942-952.

29. Wang, X., et al., *Accelerated start-up of two-chambered microbial fuel cells: Effect of anodic positive poised potential.* Electrochimica Acta, 2009. **54**(3): p. 1109-1114.

30. Pham, T.H., et al., *Improvement of Cathode Reaction of a Mediatorless Microbial Fuel Cell.* J. Microbiol. Biotechnol., 2004. **14**(2): p. 324-329.

31. Liu, H., R. Ramnarayanan, and B.E. Logan, *Production of Electricity during Wastewater Treatment Using a Single Chamber Microbial Fuel Cell.* Environ. Sci. Technol., 2004. **38**(7): p. 2281-2285.

32. Scott, K., C. Murano, and G. Rimbu, *A tubular microbial fuel cell.* Journal of Applied Electrochemistry, 2007. **37**(9): p. 1063-1068.

33. Rabaey, K., et al., *Tubular Microbial Fuel Cells for Efficient Electricity Generation.* Environmental Science & Technology, 2005. **39**(20): p. 8077-8082.

34. You, S., et al., *A graphite-granule membrane-less tubular air-cathode microbial fuel cell for power generation under continuously operational conditions.* Journal of Power Sources, 2007. **173**(1): p. 172-177.

35. He, Z., S.D. Minteer, and L.T. Angenent, *Electricity Generation from Artificial Wastewater Using an Upflow Microbial Fuel Cell.* Environ. Sci. Technol., 2005. **39**(14): p. 5262-5267.

36. He, Z., et al., *An Upflow Microbial Fuel Cell with an Interior Cathode: Assessment of the Internal Resistance by Impedance Spectrscopy.* Environ. Sci. Technol., 2006. **40**(17): p. 5212-5217.

37. Lee, H.-S., et al., *Fate of H2 in an Upflow Single-Chamber Microbial Electrolysis Cell Using a Metal-Catalyst-Free Cathode.* Environmental Science & Technology, 2009.

38. Min, B. and B.E. Logan, *Continuous Electricity Generation from Domestic Wastewater and Organic Substrates in a Flat Plate Microbial Fuel Cell.* Environmental Science & Technology, 2004. **38**(21): p. 5809-5814.

39. Liu, H. and B.E. Logan, *Electricity Generation Using an Air-Cathode Single Chamber Microbial Fuel Cell in the Presence and Absence of a Proton Exchange Membrane.* Environ. Sci. Technol., 2004. **38**(14): p. 4040-4046.

40. Cheng, S., H. Liu, and B.E. Logan, *Increased performance of single-chamber microbial fuel cells using an improved cathode structure.* Electrochemistry Communications, 2006. **8**: p. 489-494.

41. Cheng, S., H. Liu, and B.E. Logan, *Increased Power Generation in a Continuous Flow MFC with Advective Flow through the Porous Anode and Reduced Electrode Spacing.* Environ. Sci. Technol., 2006. **40**(7): p. 2426-2432.

42. Cheng, S., H. Liu, and B.E. Logan, *Power Densities Using Different Cathode Catalysts (Pt and CoTMPP) and Polymer Binders (Nafion and PTFE) in Single Chamber Microbial Fuel Cells.* Environ. Sci. Technol., 2006. **40**(1): p. 364-369.

43. Logan, B., et al., *Graphite Fiber Brush Anodes for Increased Power Production in Air-Cathode Microbial Fuel Cells.* Environmental Science & Technology, 2007. **41**(9): p. 3341-3346.

44. Liu, H., S. Cheng, and B.E. Logan, *Production of Electricity from Acetate or Butyrate Using a Single-Chamber Microbial Fuel Cell.* Environ. Sci. Technol., 2005. **39**(2): p. 658-662.

45. Catal, T., et al., *Electricity generation from polyalcohols in single-chamber microbial fuel cells.* Biosensors and Bioelectronics, 2008. **24**(4): p. 849-854.

46. Liu, H., S. Cheng, and B.E. Logan, *Power Generation in Fed-Batch Microbial Fuel Cells as a Function of Ionic Strength, Temperature, and Reactor Configuration.* Environ. Sci. Technol., 2005. **39**: p. 5488-5493.

47. Cheng, S. and B.E. Logan, *Ammonia treatment of carbon cloth anodes to enhance power generation of microbial fuel cells.* Electrochemistry Communications, 2007. **9**(3): p. 492-496.

48. Fan, Y., H. Hu, and H. Liu, *Enhanced Coulombic efficiency and power density of air-cathode microbial fuel cells with an improved cell configuration.* Journal of Power Sources, 2007. **171**(2): p. 348-354.

49. HaoYu, E., et al., *Microbial fuel cell performance with non-Pt cathode catalysts.* Journal of Power Sources, 2007. **171**(2): p. 275-281.

50. Zuo, Y., S. Cheng, and B.E. Logan, *Ion Exchange Membrane Cathodes for Scalable Microbial Fuel Cells.* Environmental Science & Technology, 2008. **42**(18): p. 6967-6972.

51. Huang, L. and B. Logan, *Electricity production from xylose in fed-batch and continuous-flow microbial fuel cells.* Applied Microbiology and Biotechnology, 2008. **80**(4): p. 655-664.

52. Feng, Y., et al., *Brewery wastewater treatment using air-cathode microbial fuel cells.* Applied Microbiology and Biotechnology, 2008. **78**(5): p. 873-880.

53. Wang, X., Y.J. Feng, and H. Lee, *Electricity production from beer brewery wastewater using single chamber microbial fuel cell.* Water Science and Technology, 2008. **57**(7): p. 1117-1121.

54. Scott, K., et al., *Application of modified carbon anodes in microbial fuel cells.* Process Safety and Environmental Protection, 2007. **85**(B5): p. 481-488.

55. Huang, L. and B. Logan, *Electricity generation and treatment of paper recycling wastewater using a microbial fuel cell.* Applied Microbiology and Biotechnology, 2008. **80**(2): p. 349-355.

56. Kim, J.R., et al., *Removal of Odors from Swine Wastewater by Using Microbial Fuel Cells.* Applied Environmental Microbiology, 2008. **74**(8): p. 2540-2543.

57. Association, A.P.H., et al., *Standard methods for the examination of water and wastewater*. 18th ed. 1992, Washington, D.C.

58. Sen, S. and I.K. Puri, *Flame synthesis of carbon nanofibres and nanofibre composites containing encapsulated metal particles.* Nanotechnology, 2004. **15**(3): p. 264-268.

59. Bae, W. and B.E. Rittmann, *A structured model of dual-limitation kinetics.* Biotechnology and Bioengineering, 1996. **49**(6): p. 683-689.

60. Chapra, S.C. and R.P. Canale, *Numerical Methods for Engineers: With Software and Programming Applications*. 4th ed. 2001: McGraw-Hill. 926.

61. *The Handbook of Water and Wastewater Microbiology*, ed. D. Mara and N. Horan. 2003, London: Academic Press. 832.

62. Rittmann, B.E. and P.L. McCarty, *Environmental Biotechnology: Principles and Applications*. 2001, New York: McGraw-Hill.

63. Lide, D.R., *CRC Handbook of Chemistry and Physics*. 89th ed. 2008-2009, Cleveland: CRC Press.

64. Hu, Z., *Electrochemical determination of anaerobic microbial decay coefficients.* Chemosphere, 2008. **72**(2): p. 312-318.

65. Cox, C.D., *Statistical Distributions of Uncertainty and Variability in Activated Sludge Model Parameters.* Water Environment Research, 2004. **76**: p. 2672-2685.

APPENDIX A EXPERIMENTAL GLUCOSE DATA

The following tables summarize the glucose concentrations measured during the fed-batch experiments in this study.

Table A.1. Laboratory Sludge Experiment Trial 1 Glucose Data

Date*	Cell No.	Anode Type [a,b]	Glucose Concentration (mg L^{-1})
7/8	1	SSM	78
7/8	2	SSM	88
7/8	3	CNS	72
7/8	4	CNS	110
7/8 A	1	SSM	1200
7/8 A	2	SSM	1300
7/8 A	3	CNS	1200
7/8 A	4	CNS	1500

***An "A" after the date denotes a sample taken after the addition of supplemental glucose**
[a] SSM = uncoated stainless steel mesh anode; [b] CNS = carbon nanostructure-coated stainless steel mesh anode

Table A.2. Laboratory Sludge Experiment Trial 2 Glucose Data

Date*	Cell No.	Anode Type [a,b]	Glucose Concentration (mg L^{-1})
8/17	1	SSM	900
8/17	2	CNS	540
8/17	3	SSM	1000
8/17	4	CNS	450
8/18	1	SSM	32
8/18	2	CNS	41
8/18	3	SSM	36
8/18	4	CNS	51
8/19	1	SSM	39
8/19	2	CNS	37
8/19	3	SSM	38
8/19	4	CNS	29
8/19 A	1	SSM	340
8/19 A	2	CNS	680

Date*	Cell No.	Anode Type [a,b]	Glucose Concentration (mg L^{-1})
8/19 A	3	SSM	740
8/19 A	4	CNS	550
8/20	1	SSM	46
8/20	2	CNS	55
8/20	3	SSM	52
8/20	4	CNS	38
8/21	1	SSM	61
8/21	2	CNS	80
8/21	3	SSM	72
8/21	4	CNS	61
8/21 A	1	SSM	550
8/21 A	2	CNS	480
8/21 A	3	SSM	690
8/21 A	4	CNS	570
8/22	1	SSM	39
8/22	2	CNS	49
8/22	3	SSM	52
8/22	4	CNS	43
8/23	1	SSM	60
8/23	2	CNS	55
8/23	3	SSM	65
8/23	4	CNS	35
8/23 A	1	SSM	630
8/23 A	2	CNS	330
8/23 A	3	SSM	340
8/23 A	4	CNS	460

***An "A" after the date denotes a sample taken after the addition of supplemental glucose**
[a] SSM = uncoated stainless steel mesh anode; [b] CNS = carbon nanostructure-coated stainless steel mesh anode

Table A.3. Sodium Azide Experiment Glucose Data

Date*	Cell No.	Anode Type [a,b]	Glucose Concentration (mg L^{-1})
3/24	1	CNS	430
3/24	2	CNS	560
3/24	3	CNS	630
3/24	4	CNS	500
3/26	1	CNS	32
3/26	2	CNS	30
3/26	3	CNS	39
3/26	4	CNS	40
3/26 A	1	CNS	250

Date*	Cell No.	Anode Type [a,b]	Glucose Concentration (mg L^{-1})
3/26 A	2	CNS	390
3/26 A	3	CNS	700
3/26 A	4	CNS	880
3/27	1	CNS	46
3/27	2	CNS	24
3/27	3	CNS	33
3/27	4	CNS	34
3/28	1	CNS	64
3/28	2	CNS	21
3/28	3	CNS	54
3/28	4	CNS	28
3/28 A	1	CNS	420
3/28 A	2	CNS	440
3/28 A	3	CNS	850
3/28 A	4	CNS	680
3/29	1	CNS	10
3/29	2	CNS	8.0
3/29	3	CNS	23
3/29	4	CNS	42
3/30	1	CNS	12
3/30	2	CNS	8.0
3/30	3	CNS	60
3/30	4	CNS	44
3/30 A	1	CNS	81
3/30 A	2	CNS	100
3/30 A	3	CNS	250
3/30 A	4	CNS	130

***An "A" after the date denotes a sample taken after the addition of supplemental glucose**
[a] SSM = uncoated stainless steel mesh anode; [b] CNS = carbon nanostructure-coated stainless steel mesh anode

Table A.4. Iron-Rich vs. Control Media Experiment Glucose Data

Date*	Cell No.	Anode Type [a,b]	Glucose Concentration (mg L^{-1})
4/21	1	CNS	1500
4/21	2	CNS	860
4/21	3	CNS	780
4/21	4	CNS	2700
4/21	5	CNS	2000
4/21	6	CNS	1500
4/22	1	CNS	45

Date*	Cell No.	Anode Type [a,b]	Glucose Concentration (mg L^{-1})
4/22	2	CNS	110
4/22	3	CNS	77
4/22	4	CNS	74
4/22	5	CNS	100
4/22	6	CNS	56
4/23	1	CNS	33
4/23	2	CNS	57
4/23	3	CNS	71
4/23	4	CNS	54
4/23	5	CNS	54
4/23	6	CNS	31
4/23 A	1	CNS	620
4/23 A	2	CNS	690
4/23 A	3	CNS	860
4/23 A	4	CNS	1000
4/23 A	5	CNS	1100
4/23 A	6	CNS	740
4/24	1	CNS	22
4/24	2	CNS	17
4/24	3	CNS	27
4/24	4	CNS	59
4/24	5	CNS	68
4/24	6	CNS	68
4/26	1	CNS	36
4/26	2	CNS	51
4/26	3	CNS	38
4/26	4	CNS	25
4/26	5	CNS	22
4/26	6	CNS	38
4/26 A	1	CNS	440
4/26 A	2	CNS	470
4/26 A	3	CNS	400
4/26 A	4	CNS	590
4/26 A	5	CNS	190
4/26 A	6	CNS	380
4/27	1	CNS	85
4/27	2	CNS	63
4/27	3	CNS	84
4/27	4	CNS	90
4/27	5	CNS	100
4/27	6	CNS	91
4/28	1	CNS	40
4/28	2	CNS	92
4/28	3	CNS	50

Date*	Cell No.	Anode Type [a,b]	Glucose Concentration (mg L^{-1})
4/28	4	CNS	66
4/28	5	CNS	81
4/28	6	CNS	47
4/29	1	CNS	41
4/29	2	CNS	53
4/29	3	CNS	54
4/29	4	CNS	48
4/29	5	CNS	120
4/29	6	CNS	--
4/29 A	1	CNS	950
4/29 A	2	CNS	700
4/29 A	3	CNS	1000
4/29 A	4	CNS	1000
4/29 A	5	CNS	400
4/29 A	6	CNS	850
4/30	1	CNS	23
4/30	2	CNS	36
4/30	3	CNS	28
4/30	4	CNS	82
4/30	5	CNS	110
4/30	6	CNS	120

***An "A" after the date denotes a sample taken after the addition of supplemental glucose**
[a] SSM = uncoated stainless steel mesh anode; [b] CNS = carbon nanostructure-coated stainless steel mesh anode

Table A.5. Low-Iron, 3% Sludge Experiment Glucose Data

Date*	Cell No.	Anode Type [a,b]	Glucose Concentration (mg L^{-1})
5/13	1	CNS	1200
5/13	2	SSM	1000
5/13	3	CNS	790
5/13	4	SSM	1300
5/13	5	CNS	2300
5/13	6	SSM	1900
5/14	1	CNS	40
5/14	2	SSM	36
5/14	3	CNS	32
5/14	4	SSM	35
5/14	5	CNS	37
5/14	6	SSM	42
5/15	1	CNS	24

Date*	Cell No.	Anode Type [a,b]	Glucose Concentration (mg L^{-1})
5/15	2	SSM	28
5/15	3	CNS	36
5/15	4	SSM	29
5/15	5	CNS	44
5/15	6	SSM	30
5/15 A	1	CNS	460
5/15 A	2	SSM	350
5/15 A	3	CNS	410
5/15 A	4	SSM	530
5/15 A	5	CNS	660
5/15 A	6	SSM	240
5/16	1	CNS	46
5/16	2	SSM	53
5/16	3	CNS	61
5/16	4	SSM	60
5/16	5	CNS	96
5/16	6	SSM	68
5/17	1	CNS	68
5/17	2	SSM	130
5/17	3	CNS	38
5/17	4	SSM	420
5/17	5	CNS	90
5/17	6	SSM	61
5/17 A	1	CNS	520
5/17 A	2	SSM	600
5/17 A	3	CNS	490
5/17 A	4	SSM	82
5/17 A	5	CNS	560
5/17 A	6	SSM	620
5/18	1	CNS	62
5/18	2	SSM	53
5/18	3	CNS	90
5/18	4	SSM	110
5/18	5	CNS	130
5/18	6	SSM	82
5/19	1	CNS	740
5/19	2	SSM	780
5/19	3	CNS	1000
5/19	4	SSM	1300
5/19	5	CNS	1300
5/19	6	SSM	410
5/19 A	1	CNS	150
5/19 A	2	SSM	230
5/19 A	3	CNS	79

Date*	Cell No.	Anode Type [a,b]	Glucose Concentration (mg L^{-1})
5/19 A	4	SSM	170
5/19 A	5	CNS	150
5/19 A	6	SSM	220
5/20	1	CNS	49
5/20	2	SSM	50
5/20	3	CNS	110
5/20	4	SSM	120
5/20	5	CNS	57
5/20	6	SSM	36

***An "A" after the date denotes a sample taken after the addition of supplemental glucose**

[a] SSM = uncoated stainless steel mesh anode; [b] CNS = carbon nanostructure-coated stainless steel mesh anode

APPENDIX B NUMERICAL MODELING SIMULATIONS

B.1 MARCUS ET AL. MODEL

The following modeling results were generated using parameters listed in the Marcus paper (with acetate as the electron donor). The model was run to check the accuracy of the code used in this study.

Table B.1. Modeling Parameters.

Parameter	Symbol	Value	Units
Electron equivalence of glucose	γ_1	8.0	mmol e^- mmol-ac^{-1}
Electron equivalence of active biomass	γ_2	0.177	mmol e^- mg-VSS^{-1}
Glucose diffusion coefficient	$D_{ED,l}$	0.941	cm^2 day^{-1}
Glucose diffusion coefficient in biofilm	$D_{ED,f}$	0.753	cm^2 day^{-1}
Half-max-rate glucose concentration	K_{sd}	3.0×10^{-5}	mmol cm^{-3}
Bulk liquid electron donor concentration	$S_{d,bulk}$	3.0×10^{-4}	mmol cm^{-3}
Maximum specific rate of ED utilization	q_{max}	0.132	mmol-ac mg-VSS^{-1} day^{-1}
True yield	Y	4.52	mg-VSS mmol-ac^{-1}
Inactivation decay coefficient for active biomass	b_{ina}	0.05	day^{-1}
Endogenous decay coefficient for active biomass	b_{res}	0.05	day^{-1}
Rate of biomass loss due to detachment	b_{det}	0.05	day^{-1}
Fraction of electrons from glucose used for energy generation	fe^0	0.90	--
Density of active biomass	$X_{f,a}$	200	mg-VSS cm^{-3}
Density of inactive biomass	$X_{f,i}$	200	mg-VSS cm^{-3}
Conductivity of biofilm matrix	k_{bio}	0.0001	mS cm^{-1}
Anode potential	V_{anode}	0.50	V

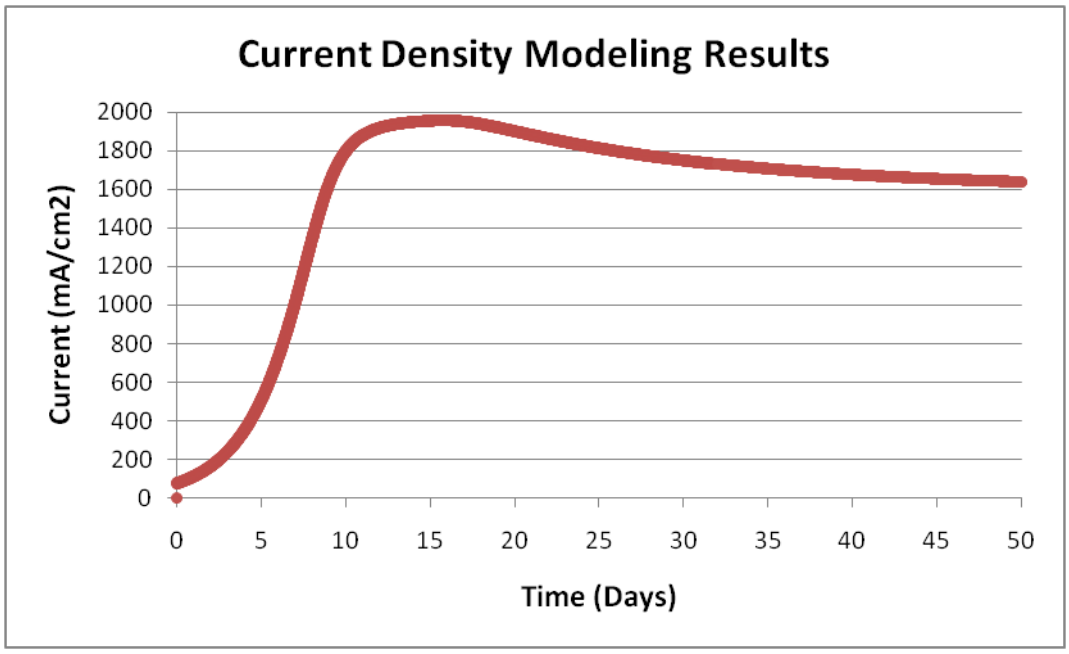

Figure B.1. Current density modeling results using acetate.

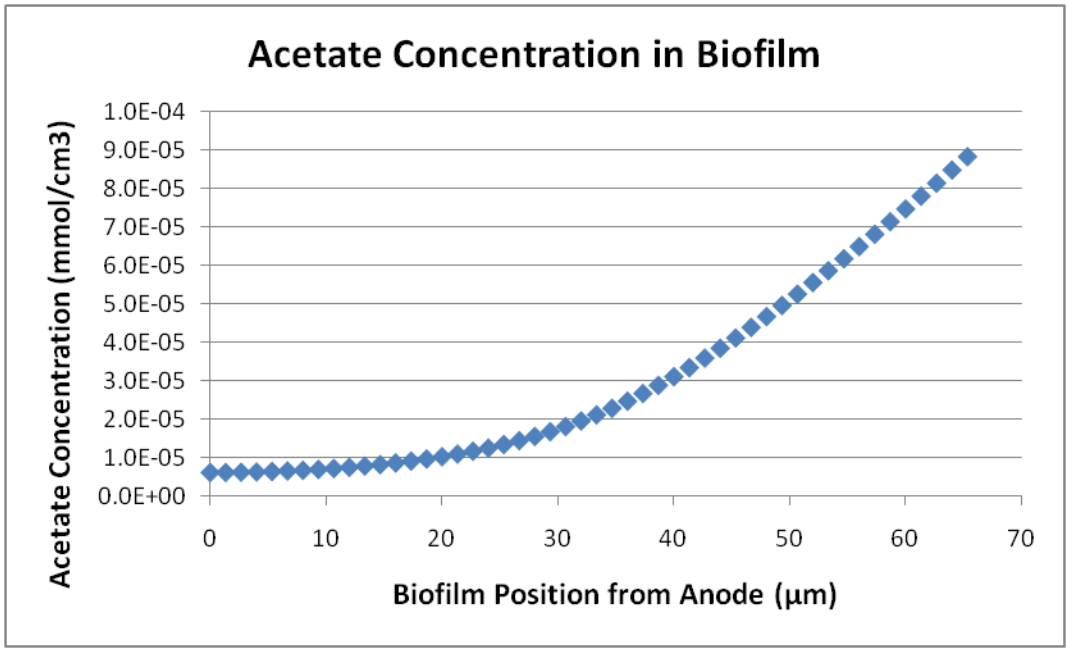

Figure B.2. Acetate concentration in biofilm at day 50.

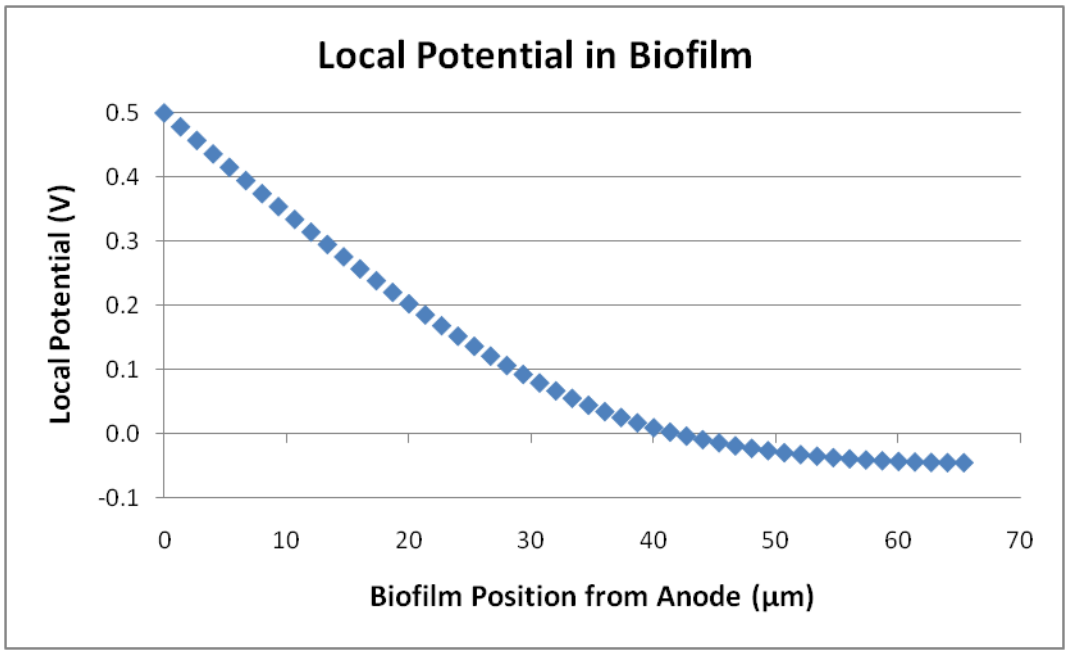

Figure B.3. Local potential in biofilm at day 50.

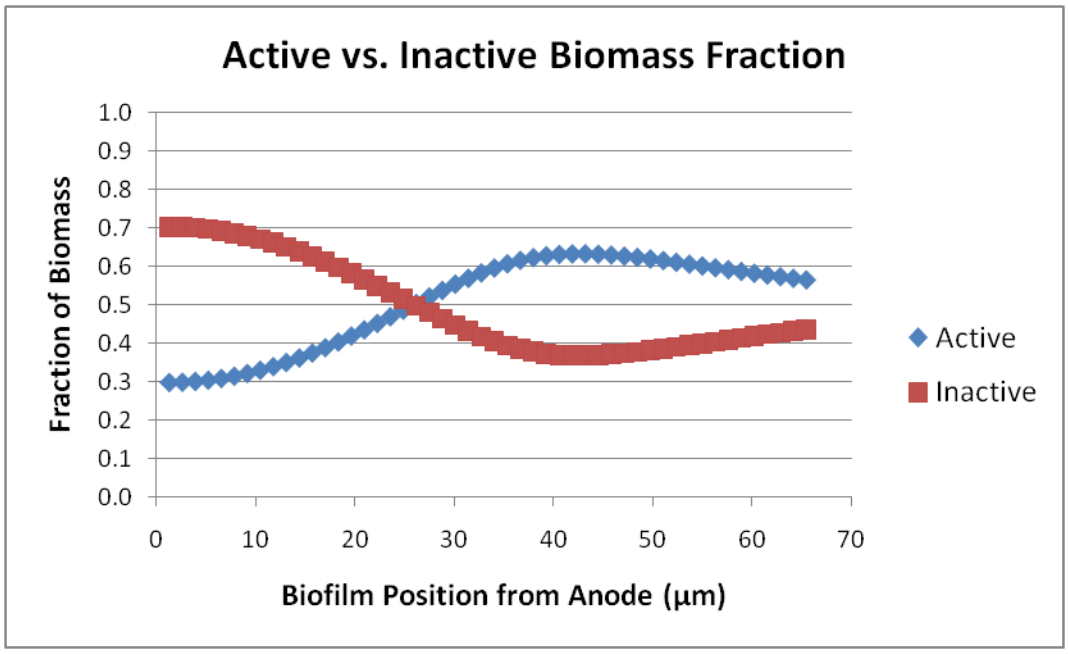

Figure B.4. Active and inactive biomass fractions in biofilm at day 50.

B.2 BIOFILM CONDUCTIVITY SENSITIVITY

Using a q_{max} value of 0.090 mmol-gl mg-VSS^{-1} day^{-1} and the other parameters outlined in **Table 5.5**, the numerical model was run for high (0.001 mS cm^{-1}) and low (0.00001 mS cm^{-1}) values of biofilm conductivity (κ_{bio}). The results for current density are given below in **Figure B.5**.

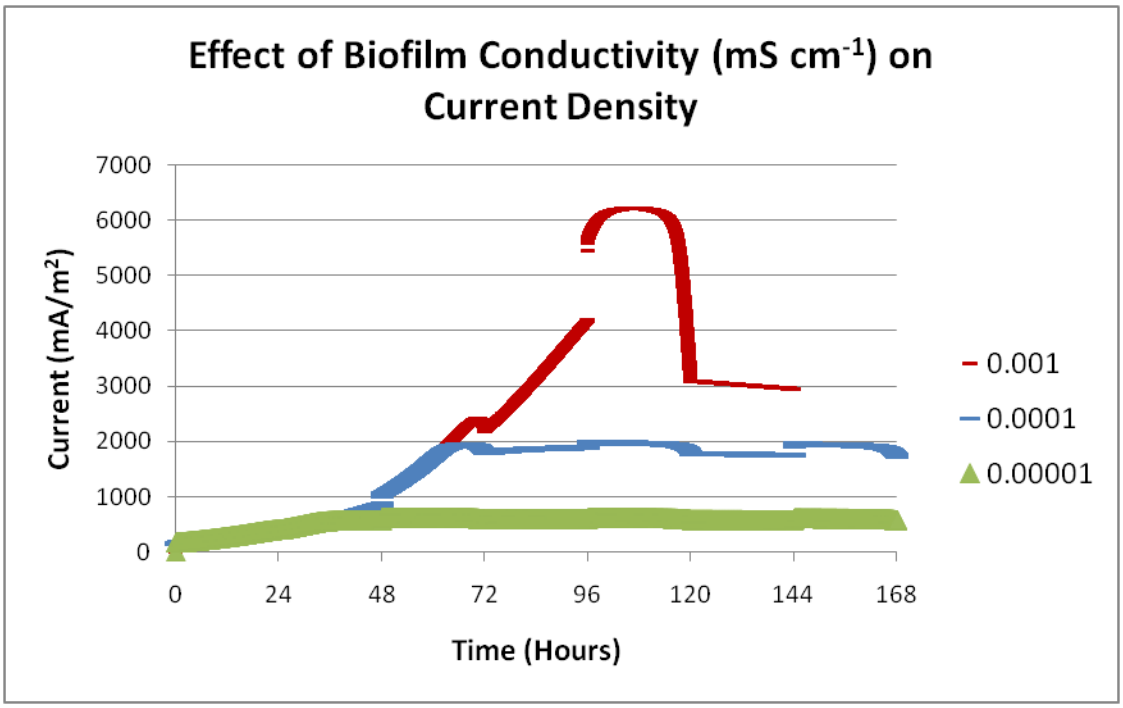

Figure B.5. Effect of biofilm conductivity on current density results from numerical model.